Asymptotic preserving automatic domain decomposition for the Vlasov-Poisson-BGK system with applications to plasmas

Giacomo Dimarco[*], Luc Mieussens[†], Vittorio Rispoli [‡§]

Abstract

In this work we present an efficient strategy to deal with plasma physics simulations in which localized departures from thermodynamical equilibrium are present. The method relies on the introduction of buffer zones which realize a smooth transition between the kinetic and the fluid regions. In this paper we extend the idea, recently developed in [13, 14], of dynamic coupling and of buffer zones to the case of plasmas. The basic idea consists in using an hybrid scheme in which both kinetic and fluid descriptions are considered and coupled together. Moreover, we construct our scheme in order to solve the kinetic model by asymptotic preserving and accurate methods which permit to get high efficiency while guaranteeing precision of the proposed scheme for all regimes. The numerical scheme is validated and its performances are analyzed by numerical simulations.

Keywords: Kinetic-fluid coupling, Vlasov-BGK-Poisson system, plasmas simulations, Asymptotic Preservation, Asymptotic Accuracy.

Acknowledgments:

1 Introduction

Computer simulations are very powerful and useful tools for advanced research in both industry and academy. Apart from old but still very important fields of application, cutting edge areas of modern technology exploit their great potential like nanotechnology, biomedicine and semiconductors or plasma industries just to name a few. The most widely used physical models in these fields are both fluid systems, such as compressible Euler or Navier-Stokes equations, and kinetic equations, such as those of Boltzmann or Vlasov type [10]. Latter descriptions are more precise in representing the physics of various phenomena but unfortunately solving kinetic equations has in general a prohibitive cost in terms of computational power and memory storage and, thus, simplified models are often used.

In this paper, we develop a general numerical method for the solution of plasma physics models. Our aim is to design a scheme which has at least second order of accuracy and is at the same time efficient in term of computational and memory storage costs, in order to be used for real life applications. Indeed, both requirements on efficiency are of paramount importance for realistic simulations which are, in general, modeled by large dimensional systems.

Typical examples of possible applications include simulations of plasmas produced around hypersonic bodies, ion wind of corona discharges and magnetic fusion processes. Plasma dynamics is characterized by a wide range of spatial and temporal scales. Depending on conditions, macroscopic Euler-like systems or

[*]Institut de Mathématiques de Toulouse, Toulouse, France. giacomo.dimarco@math.univ-toulouse.fr

[†]Institut de Mathématiques de Bordeaux, TALENCE cedex France. Luc.Mieussens@math.u-bordeaux1.fr

[‡]Department of Mathematics, University of Ferrara, Italy. rspvtr@unife.it

[§]The author is partially supported by "Programma Giovani Ricercatori 2012", Gruppo Nazionale per il Calcolo Scientico (GNCS) - Indam.

kinetic equations of Boltzmann type are commonly used for describing these problems. The most widely used kinetic model is the Vlasov equation for the particles constituting the plasma, usually coupled with a Poisson equation for the electric potential or, more generally, through Maxwell equations to include also magnetic and electromagnetic effects. When collisions between particles are also taken into account, we refer to it as the collisional Vlasov model. In this work we consider this last kind of problems, modeling collisions by a relaxation towards the thermodynamical equilibrium and we refer to such description as the Vlasov-BGK model. It is well known that, when sufficiently close to equilibrium, kinetic descriptions can be replaced by Euler or Navier-Stokes based models, also coupled with Poisson or Maxwell equations. Even if fluid models are sufficiently accurate to describe many observed phenomena, for some of them this choice is inadequate. In such cases, it turns out that a kinetic description is strictly necessary to correctly represent the solutions.

The most widely used numerical methods when dealing with the full kinetic Vlasov equation are Particle-In-Cell (PIC) approaches [7]. They have many advantages in terms of computational cost especially for large dimensional problems, they are capable of easily enforcing physical properties such as conservation laws while, when handling with complex geometries, they maintain large flexibility. On the other hand, these methods involve a significant level of numerical noise and the convergence rate is slow, typically they converge proportionally with the square root of the number of sample. Moreover, in situations close to thermodynamical equilibrium the number of collisions increases and thus PIC methods or, more in general, direct Monte Carlo simulations becomes rapidly inefficient.

For this reason, domain decomposition techniques have been proposed in the recent past, see [1, 15, 13, 14, 31, 41]. In many practical situations the resolution of the kinetic equations is required only in small zones where the departure from thermodynamical equilibrium is large, like near shock layers or where the electric field is strong, while inside the rest of the computational domain the microscopic description is unnecessary because a fluid system would also provide sufficiently accurate solutions.

In this paper we precisely address the above situation. The general framework for the construction of coupling kinetic-fluid schemes involves three main problems: the first one is how to define proper criteria in order to identify departure from equilibrium states and breakdown of fluid models, the second main problem is how to mathematically realize the coupling in other words how to treat the interfaces and the third one is the choice of the appropriate numerical methods for solving the macroscopic and the microscopic equations. For the first issue we refer, for instance, to [34, 44, 43] in which various breakdown criteria have been analyzed; we describe in the following how we choose to handle this issue in our scheme. Concerning the second point, the main difficulties come from the match of the two models at the interfaces. Several different ideas are described in the works [2, 8, 40]. We recall that the decomposition between equilibrium and non equilibrium states can be realized also in velocity space instead of in physical space, see for instance [11, 17]. It is also important to stress that most of the mentioned methods use a static interface between kinetic and fluid regions but this approach is inadequate and inefficient for many realistic problems and, for this reason, more recently automatic domain decomposition methods have also been developed [13, 14]. The third problem, the choice of the appropriate numerical methods, can be solved in different ways. A first possibility is given by finite volumes based deterministic-deterministic methods, such as for instance in [15, 13, 14]. A second approach consists in using particle-particle methods [42], which provide a simple solution to the interface problem. On the other hand, their solutions contain large statistical errors which are typical drawbacks of Monte Carlo methods. A third approach is the deterministic-particle approach in which finite volume methods are used for the fluid model while the kinetic model is solved using Direct Simulation Monte Carlo method. For a description of advantages, drawbacks, recent results and more references for this last approach we refer to [39, 40].

Here, we propose a fully deterministic finite volume-finite volume numerical method for the resolution of the collisional Vlasov equation coupled with the compressible Euler system and with the Poisson equation for the electric potential, i.e. the Vlasov-Euler-Poisson model, based on a dynamic domain decomposition technique. One of the key point of the domain decomposition method relies in the introduction of a buffer zone in which the transition from one model to the other and vice-versa is gradual. Therefore, inside

buffer zones both models are solved and the solution of the full problem is obtained as the combination of the kinetic and of the fluid solutions. The introduction of the intermediate zone makes each of the models degenerate at the borders and so in this way no interface conditions are needed. The decomposition of the domain is dynamic, or adaptive, in the sense that it applies everywhere in the domain the suited model following the time evolution of the system. For this reason we consider an evolution equation also for the coupling function. The present work is an extension of two earlier works [15, 13] in which the coupling of the Boltzmann-BGK equation and of the compressible Euler system was studied. Here we also extend the results obtained in [16] for plasmas where the Vlasov-Poisson-BGK and the Euler-Poisson coupling was studied assuming a constant in time coupling function. The second key point of the proposed method relies on the use of Asymptotic Preserving (AP) and Accurate (AA) schemes for solving the Vlasov-BGK equation. This is crucial point since we are considering at the same time different regimes in different spatial regions and thus we may have to solve the Vlasov-BGK equation close to the fluid regime, which is usually a real challenge if non appropriated numerical methods are used.

In dense regimes, in fact, the collision rate grows exponentially and the collisional time becomes very small. In such situations, standard computational approaches lose their efficiency due to the necessity of using very small time steps in deterministic schemes or, equivalently, a large number of collisions in probabilistic approaches. On the other hand, the time scale of the evolution is the slower fluid dynamic one, which can be much larger than the one determined from the collision scale this means that we would like to relate our time step restriction only to the slow scale.

To solve this problem we choose to construct our method using the so-called AP ([27, 28, 29, 32, 38]) and AA ([20]) discretizations for the collisional Vlasov equation. These schemes automatically reduce to a consistent numerical approximations of the relevant macroscopic model when the scaling parameter of the system goes to zero. Thanks to the use of this strategy we can solve the kinetic equation, in the regions of the domain where it is needed, using a discretization which is consistent with that for the macroscopic model and this is fundamental for the coupling of the two solvers. We also adopt proper numerical strategies thanks to which we overcome the strong time step restriction caused by the stiff character of the collision term. In this way we are able to greatly decrease the computational cost of the simulations and while still achieving high resolution in time and space independently on the regime.

We explain in details our choices in the rest of the paper, which is organized as follows. Next section is devoted to the description of the mathematical model: we introduce the Vlasov-BGK equation, its properties and the limiting model. In section 3 we present the coupling method and in section 4 we give the details of the proposed numerical scheme (time and phase space discretizations) of the system we want to solve which is derived by the coupling strategy. In this section we also discuss and present the technique for an efficient implementation in term of memory storage. In section 5 we describe the strategy for the determination of kinetic and hydrodynamic regions and for the updating of the coupling function. Section 6 contains numerical tests which validate the presented strategy while in the last section we summarize our work and suggest some possible future directions.

2 Vlasov-BGK-Poisson model

The problem studied in the paper is the dynamics of a two-species plasma constituted of electrons and one species of ions. This can be modeled by the two particles Vlasov-BGK-Poisson system for $f_i(x, v, t)$ and $f_e(x, v, t)$

$$\partial_t f_i + v \cdot \nabla_x f_i + E \cdot \nabla_v f_i = \frac{1}{\varepsilon_i}(M_{f_i} - f_i), \tag{1}$$

$$\partial_t f_e + v \cdot \nabla_x f_e - m_r E \cdot \nabla_v f_e = \frac{1}{\varepsilon_e}(M_{f_e} - f_e), \tag{2}$$

complemented by the initial condition

$$f_{i,e}(x, v, t = 0) = f_{i,e,0}(x, v). \tag{3}$$

Variables $f_{i,e} = f_{i,e}(x, v, t)$ are non negative functions describing the time evolution of particles distributions depending on the position variable $x \in \Omega \subset \mathbb{R}^d$, on the velocity variable $v \in \mathbb{R}^d$ and on time $t > 0$. Constant $m_r = m_i/m_e$ is the mass ratio of the two particles. The symbol d indicates the dimension of the velocity and of the physical space and it can take the values $d = 1, 2$ or 3. Collisions are modeled by a relaxation towards the local thermodynamical equilibrium defined by the maxwellian distribution function $M_{f_{i,e}}$. In this work we assume that the local equilibrium is computed independently for the two different particles, i.e. every species tends to its own equilibrium state. In many cases such assumption is not a strong restriction. However, global equilibrium states for electrons and ions can be defined as well, which leads to different models and thus to different discretizations.

For all the rest of the paper, when no confusion can be made and when the definitions or the properties concern both distributions (for ions and electrons), we will omit the subscripts i and e. We write formulas and properties for ions, observing that those for electrons can be obtained simply changing the sign of the electric field and multiplying by the mass ratio; we will highlight any situation in which this will not be the case. Parameter $\varepsilon > 0$ in the Vlasov-BGK equation represents the Knudsen number which is proportional to the mean free path between two collisions. The local maxwellian functions depend on $f_{i,e}$ through their moments and they are defined by (we omit the subscripts)

$$M_f = M_f[\rho, u, T](v) = \frac{\rho}{(2\pi T)^{d/2}} \exp\left(\frac{-|u - v|^2}{2T}\right),$$

where ρ, u and T are density, mean velocity and temperature of the ions respectively of the electrons defined by

$$\rho = \int_{\mathbb{R}^d} f \, dv, \qquad u = \frac{1}{\rho} \int_{\mathbb{R}^d} v f \, dv, \qquad T = \frac{1}{d\rho} \int_{\mathbb{R}^d} |v - u|^2 f \, dv.$$

The energy $\mathcal{E}$ is defined as

$$\mathcal{E} = \int_{\mathbb{R}^d} \frac{|v|^2}{2} f \, dv = \frac{1}{2}\rho|u|^2 + \frac{d}{2}\rho T.$$

The maxwellian distributions M_f can be characterized as the unique solutions of the following entropy minimization problems for each species

$$H(M_f) = \min\{H(f), \ f \geq 0 \ s.t. \int_{\mathbb{R}^d} \boldsymbol{m} f \, dv = \boldsymbol{\varrho}\} \tag{4}$$

where H is the kinetic entropy of f

$$H(f) = \int_{\mathbb{R}^d} f \log f dv,$$

$\boldsymbol{m}$ is the vector containing collision invariants and $\boldsymbol{\varrho}$ contains the first three moments of f, respectively given by

$$\boldsymbol{m}(v) = (1, v, |v|^2/2)^t \qquad \text{and} \qquad \boldsymbol{\varrho} = (\rho, \rho u, \mathcal{E})^t.$$

This is the well-known local Gibbs principle which expresses the fact that the local thermodynamical equilibrium state minimizes, in the mathematical sense, the entropy among all possible states subject to the constraint that its moments $\boldsymbol{\varrho}$ are prescribed. Next, we will use a discretized version of the above principle to define a discretized equilibrium function.

Finally, E represents the electric field which is obtained as $E = -\nabla_x \phi$, where ϕ is a self consistently determined electric potential. The latter is obtained as the solution of the following Poisson equation

$$-\lambda^2 \Delta \phi = \rho_i - \rho_e \tag{5}$$

with λ the so-called Debye length.

In order to derive macroscopic equations, we multiply the Vlasov-BGK equation (1) by the collision invariants $\boldsymbol{m}$ and we integrate with respect to v. If considering electrons, we would use (2) instead but

the procedure is identical. We obtain a system of non-closed balance laws for the macroscopic quantities $\boldsymbol{\varrho}$ since the closure involves higher order moments of the distribution function than only ρ, ρu and $\mathcal{E}$. As $\varepsilon \to 0$ the distribution f tends, at least formally, to the local maxwellian and in this limit it is possible to close the moments system and get an Euler-like system of equations which reads

$$\begin{aligned} \partial_t \rho + \nabla_x \cdot (\rho u) &= 0, \\ \partial_t (\rho u) + \nabla_x \cdot (\rho u \otimes u + pI) &= \rho E, \\ \partial_t \mathcal{E} + \nabla_x \cdot ((\mathcal{E} + p)u) &= \rho u E, \\ p = \rho T, \qquad \mathcal{E} &= \frac{1}{2}\rho |u|^2 + \frac{d}{2}\rho T, \end{aligned} \tag{6}$$

with p the pressure. For electrons, a similar system can be derived as previously described, i.e. simply changing the sign and multiplying by the mass ratio terms containing the electric field. We also recall the first order correction with respect to ε of the compressible Euler equations which will be useful in the following to define breakdown criteria. Such correction is nothing else but a Compressible Navier-Stokes like (CNS) system

$$\begin{aligned} \partial_t \rho + \nabla_x \cdot (\rho u) &= 0, \\ \partial_t (\rho u) + \nabla_x \cdot (\rho u \otimes u + pI) &= \rho E - \nabla_x \cdot (\varepsilon \sigma), \\ \partial_t \mathcal{E} + \nabla_x \cdot ((\mathcal{E} + p)u) &= \rho u E - \nabla_x \cdot (\varepsilon \sigma u + q), \end{aligned} \tag{7}$$

where the stress tensor σ is given by $\sigma = -\mu\Big(\nabla_x u + (\nabla_x u)^t - \frac{2}{d}\nabla_x \cdot u I\Big)$ while the heat flux is given by $q = -\varepsilon\kappa\nabla_x T$. In these relations the viscosity μ and the heat conductivity κ are functions of the first three moments $\boldsymbol{\varrho}$, see for instance [4] and the references therein for more details.

3 The coupling method

In order to simplify notations, we now describe the coupling strategy using only equations for ions. Exactly the same algorithm is used for electrons and for multi species plasmas.

3.1 Decomposition of the Vlasov-BGK equation

We introduce a splitting of the domain Ω into three non overlapping subsets $\mathcal{B}_t^K \cup \mathcal{B}_t^H \cup \mathcal{B}_t = \Omega$ depending on time t and we define a cut-off function $h = h(x,t)$, continuous on Ω and such that

$$h(x,t) = \begin{cases} 1 & \text{if } x \in \mathcal{B}_t^K \\ 0 & \text{if } x \in \mathcal{B}_t^H \\ 0 \le h(x,t) \le 1 & \text{if } x \in \mathcal{B}_t. \end{cases}$$

Then we define two new distribution functions $f_K = hf$ and $f_H = (1-h)f$ and we study their time evolution, instead of that of f. We have

$$\begin{aligned} \partial_t f_K &= \partial_t (hf) = f\,\partial_t h + h\partial_t f, \\ \partial_t f_H &= \partial_t \Big((1-h)f\Big) = -f\,\partial_t h + (1-h)\partial_t f. \end{aligned}$$

Using the Vlasov-BGK equation (1) we get for f_K and f_H

$$\begin{aligned} \partial_t f_K &= f\,\partial_t h + h\Big(- v \cdot \nabla_x f - E \cdot \nabla_v f + \frac{1}{\varepsilon}(M_f - f)\Big), \\ \partial_t f_H &= -f\,\partial_t h + (1-h)\Big(- v \cdot \nabla_x f - E \cdot \nabla_v f + \frac{1}{\varepsilon}(M_f - f)\Big). \end{aligned}$$

Observing moreover that $f = f_K + f_H$ finally leads to the following system for f_K and f_H

$$\partial_t f_K + h\, v \cdot \nabla_x f_K + h\, v \cdot \nabla_x f_H + E \cdot \nabla_v f_K = \frac{h}{\varepsilon}\Big(M_f - f\Big) + f\partial_t h, \tag{8}$$

$$\partial_t f_H + (1-h)\, v \cdot \nabla_x f_H + (1-h)\, v \cdot \nabla_x f_K + E \cdot \nabla_v f_H = \frac{1-h}{\varepsilon}\Big(M_f - f\Big) - f\partial_t h, \tag{9}$$

with initial data

$$f_K(x,v,0) = h(x,0) f(x,v,0)\,, \qquad f_H(x,v,0) = (1-h(x,0)) f(x,v,0). \tag{10}$$

Note that if $f = f_K + f_H$ is the solution of (1) with initial data (3), then (f_K, f_H) is the solution of (8-9) with initial data (10) and conversely.

3.2 Kinetic-Fluid coupling

In order to exploit the kinetic-fluid coupling, the domain is subdivided into two regions: inside one of the two we suppose the distribution function to be close to the local maxwellian, which means it is close to the thermodynamical equilibrium, while inside the other we suppose it to be far from it, i.e. the system is in a kinetic regime. We choose to set $h = 0$ over the region $\mathcal{B}_t^H$ of the domain where f is close to the local maxwellian. Therefore, $f_H = f$ is close to its associated maxwellian $M_{f_H} = M_f$ and we can replace the Vlasov-BGK equation by the Euler system without making any significant error. We also suppose that f_H remains close to the equilibrium in the whole buffer zone $\mathcal{B}_t$ and thus it coincides with M_{f_H} in the entire subset $\mathcal{B}_t^H \cup \mathcal{B}_t$.

Replacing f_H by M_{f_H} in (9) and considering the hydrodynamic moments (mass, momentum and energy), leads to the following Euler like system defined for all $x \in \mathcal{B}_t^H \cup \mathcal{B}_t$

$$\begin{aligned}
&\partial_t \rho_H + (1-h)\nabla_x \cdot (\rho_H u_H) = -(1-h)\nabla_x \cdot \big(\textstyle\int_{\mathbb{R}^d} v f_K\, dv\big) - \rho \partial_t h,\\
&\partial_t (\rho_H u_H) + (1-h)\nabla_x \cdot (\rho_H u_H \otimes u_H + p_H I) = \rho_H E - (1-h)\nabla_x \cdot \big(\textstyle\int_{\mathbb{R}^d} v^2 f_K\, dv\big) - \rho u \partial_t h,\\
&\partial_t \mathcal{E}_H + (1-h)\nabla_x \cdot \Big((\mathcal{E}_H + p_H) u_H\Big) = \rho_H u_H E - (1-h)\nabla_x \cdot \Big(\textstyle\int_{\mathbb{R}^d} v \frac{|v|^2}{2} f_K\, dv\Big) - \mathcal{E}\partial_t h,
\end{aligned} \tag{11}$$

where $(\rho_H, \rho_H u_H, \mathcal{E}_H)$ are the moments associated to f_H. Initial data are defined by

$$(\rho_H, u_H, T_H)|_{(x,0)} = (1 - h|_{(x,0)})(\rho, u, T)|_{(x,0)}.$$

Under these assumptions, we have $f = f_K + M_{f_H}$ in the whole domain, with f_K being now solution of the kinetic equation

$$\partial_t f_K + h\, v \cdot \nabla_x f_K + h\, v \cdot \nabla_x M_{f_H} + E \cdot \nabla_v f_K = \frac{h}{\varepsilon}(M_f - f) + f\partial_t h \tag{12}$$

The coupling model consists in considering system (11) for the hydrodynamic moments inside the region $\mathcal{B}_t^H \cup \mathcal{B}_t$ where $f \approx M_f$ and equation (12) for the kinetic distribution function in the region $\mathcal{B}_t^K \cup \mathcal{B}_t$ where f is far from equilibrium.

When $h = 0$, system (11) coincides with system (6) because $f_K = 0$ and $f_H = M_{f_H} = M[\boldsymbol{\varrho}_H]$. Moreover no interface conditions are needed at the intersections of the different regions because each variable is directly set to zero on the boundary between the buffer and the definition domain of the other variable; More precisely, f_K is directly set to zero on the border between $\mathcal{B}_t$ and $\mathcal{B}_t^H$ and similarly for $\boldsymbol{\varrho}_H$. Inside the buffer zone $\mathcal{B}_t$ the solution of the full kinetic problem f is computed as the sum of the kinetic part f_K and of the maxwellian M_{f_H}, obtained by its moments $\boldsymbol{\varrho}_H$.

To summarize, the solution of the full kinetic-fluid problem for a one species plasma is given by

$$f = \begin{cases} f_K & \text{if } x \in \mathcal{B}_t^K \\ M_{f_H} & \text{if } x \in \mathcal{B}_t^H \\ f_K + M_{f_H} & \text{if } x \in \mathcal{B}_t. \end{cases}$$

In the case of a two species plasma, which is the one considered in this paper, the above decomposition is performed for electrons and ions independently and it can be summarized as follows

$$f_i = \begin{cases} f_{K,i} & \text{if } x \in \mathcal{B}_t^{K,i} \\ M_{f_{H,i}} & \text{if } x \in \mathcal{B}_t^{H,i} \\ f_{K,i} + M_{f_{H,i}} & \text{if } x \in \mathcal{B}_t^i \end{cases}, \qquad f_e = \begin{cases} f_{K,e} & \text{if } x \in \mathcal{B}_t^{K,e} \\ M_{f_{H,e}} & \text{if } x \in \mathcal{B}_t^{H,e} \\ f_{K,e} + M_{f_{H,e}} & \text{if } x \in \mathcal{B}_t^e. \end{cases}$$

Expressions above say that we model both electrons and ions by system (11)-(12) (changing conveniently the equations for the two species multiplying by sign and mass ratio all electric field terms). We recall that the electric potential is computed through the Poisson equation (5).

Observe that equilibrium regions for the two species can be different in the general case. We can have situations in which both electrons and ions are solved by fluid models, others in which both species are solved using a kinetic description and regions in which electrons are solved by fluid equations while ions are treated by kinetic equations and viceversa. The possibility to treat the different species independently is a very important feature of our method.

Another relevant property of the presented method is that it is possible to create new hydrodynamic, buffer and kinetic zones during the simulation and divide the domain accordingly. It is possible to define as many buffers and as many kinetic regions as necessary if the macroscopic model fails to give the correct solution in different parts of the domain, also if they are far apart from each other. We can also, on the other side, switch to the less costly macroscopic description if, during the time evolution, equilibrium is restored in some region in space. The coupling function h is updated at any time step to correctly follow the evolution of the system. At any time, it is defined as a continuous and piecewise linear function over the whole domain Ω, i.e. constant inside kinetic and hydrodynamic regions and linear over buffers. The way in which new zones are defined is detailed next.

4 Numerical approximation of the coupled model

As in previous chapter, in this section we describe the complete numerical discretization of the coupled model only for ions. This section is divided into three parts which describe the discretization in velocity, time and space variables respectively.

We design our scheme in order to be globally second order accurate in time and phase space. To accomplish this task, for both the kinetic and the hydrodynamic models we use a second order conservative scheme for hyperbolic balance laws to discretize phase space variables, i.e. space and velocity, and we use a second order Implicit-Explicit Runge-Kutta method for the time discretization. More details are given in each subsection.

4.1 Velocity discretization

In order to handle the velocity space discretization of the kinetic equation (12) we consider a Discrete Velocity Model (DVM). The principle of DVM is to set a grid in the velocity space and to transform the kinetic equation into a set of linear hyperbolic equations coupled by the source terms. Here we use this technique to discretize our coupled model and we refer to the work of Mieussens [35] for the description of this model and for more details.

Let $\mathcal{K}$ be a multi-index of $\mathbb{N}^d$, defined by $\mathcal{K} = \left\{k = (k^i)_{i=1}^d,\ 0 \le k^i \le N_v^i\right\}$, where $\{N_v^i\}$ are some given bounds. Consider also a Cartesian grid $\mathcal{V}$ of $\mathbb{R}^d$, say $\mathcal{V} = \{v_k = a_v + k\Delta v,\ k \in \mathcal{K}\}$ where $a_v \in \mathbb{R}^d$ is

an arbitrary vector and Δv is a scalar which represents the grid step in velocity space. We denote the discrete collision invariants on $\mathcal{V}$ by $\boldsymbol{m}_k = (1, v_k, \frac{1}{2}|v_k|^2)$.

In this setting, the continuous distribution function f is replaced by a $N-$vector $f_N(x,t)$, with $N = N_v^1 + \ldots + N_v^d$, whose components are approximations of f at location v_k

$$f_N(x,t) = (f_k(x,t))_k, \qquad f_k(x,t) \approx f(x, v_k, t).$$

The same notation is used for all other microscopic quantities, as for example $M_k[\boldsymbol{\varrho}]$ and $M_k[\boldsymbol{\varrho}_H]$. Fluid quantities are obtained from f_N thanks to discrete summation over $\mathcal{V}$

$$\boldsymbol{\varrho}(t,x) = \sum_k \boldsymbol{m}_k f_k(x,t)\, \Delta v.$$

Applying the DVM approximation to equation (12) we obtain

$$\partial_t f_{k,K} + h\, v_k \cdot \nabla_x f_{k,K} + h\, v_k \cdot \nabla_x \mathcal{M}_k[\boldsymbol{\varrho}_H] + E \cdot \nabla_v f_{k,K} = \frac{h}{\varepsilon}\Big(\mathcal{M}_k[\boldsymbol{\varrho}] - f_k\Big) + f_k \partial_t h, \tag{13}$$

where $f_{k,K}$ is the DVM approximation of f_K while $\mathcal{M}_k[\boldsymbol{\varrho}]$ and $\mathcal{M}_k[\boldsymbol{\varrho}_H]$ are approximations of,respectively, $M[\boldsymbol{\rho}]$ and $M[\boldsymbol{\rho}_H]$ which we describe later. Finally, f_k is the global distribution defined as in the continuous case by $f_k = f_{k,K} + \mathcal{M}_k[\boldsymbol{\varrho}_H]$.

Great care must be taken when discretizing the global maxwellian $M[\rho, u, T]$. We do not enter in details here and refer to [35, 14] for a discussion on all the issues related to such approximation. A possible way to guarantee that the (modified) numerical maxwellian $\mathcal{M}_k[\boldsymbol{\varrho}]$ shares the same moments as $M[\boldsymbol{\varrho}]$ is to define it as the (unique) solution of a suitable discrete entropy minimization problem, analogous to the continuous one described by (4), using the macroscopic moments ρ, u and T. Namely, one can show that the equilibrium distribution is given by

$$\mathcal{M}_k[\boldsymbol{\varrho}] = \exp(\boldsymbol{\alpha}(\boldsymbol{\varrho}) \cdot \boldsymbol{m}_k),$$

where $\boldsymbol{\alpha}(\boldsymbol{\varrho})$ is solution of the following non linear problem

$$\sum_k \boldsymbol{m}_k \exp(\boldsymbol{\alpha}(\boldsymbol{\varrho}) \cdot \boldsymbol{m}_k)\, \Delta v = \boldsymbol{\varrho}.$$

These equations are practically solved by an iterative Newton algorithm. The same problem is solved for finding $\mathcal{M}_k[\boldsymbol{\varrho}_H]$, starting from hydrodynamic moments $\boldsymbol{\varrho}_H$. A complete numerical study (existence, uniqueness, convergence) regarding the DVM method and the technique for finding the modified equilibrium distribution can be found in [35, 36].

4.2 Time discretization

The time discretization plays a crucial role when treating multiscale problems. In fact, the changing from the microscopic to the macroscopic description ad viceversa leads to very challenging numerical difficulties.

The main issue is that we want to use the same time and space discretization at any time for the whole domain, i.e. without knowing or caring if the system is described by macroscopic or by microscopic models. We want our numerical scheme to be consistent and accurate with both kinetic equations and limiting Euler-like systems. A related problem is that when the mean free path goes to zero, i.e. $\varepsilon \to 0$, the collision operator of the kinetic equation becomes stiff, this makes classical numerical methods prohibitively expensive. We solve this problem by deriving a high order time discretization which overcomes the stiff character of the problem and which leads to an accurate and efficient scheme with a time step restriction independent from the Knudsen number ε. We now detail all the step concerning the time discretization.

The time discretization should satisfy two important properties, commonly known as Asymptotic Preservation (AP) and Asymptotic Accuracy (AA). They guarantee, respectively, a stability condition and a uniform order of accuracy for the time discretization independently from the scaling parameter ε. We recall the two definitions for the original Vlasov-BGK equation

AP: *a consistent time discretization method for (1) of step-size Δt is asymptotic preserving (AP) if, independently of the initial data and of the step-size Δt, in the limit $\varepsilon \to 0$ it becomes a consistent time discretization method for system (6).*

AA: *a consistent time discretization method for (1) of step-size Δt is asymptotically accurate (AA) if, independently of the initial data and of the step-size Δt, the order of accuracy is preserved for all choices of ε.*

The same definitions are valid for electrons, considering equation (2) instead of (1). Observe that the above requirements imply that in the limit when $\varepsilon = 0$ the numerical discretization is automatically reduced to a consistent scheme for the corresponding macroscopic model which, in addition, preserves the desired order of accuracy for any value of the scaling parameter ε. For more details regarding AP schemes we refer to [27, 12, 32, 37, 5, 21, 22] while for AA schemes to [18, 18, 19, 20].

In order to ensure the AP and AA properties for our scheme and also to avoid the severe time step restriction due to collisions, we choose to use IMplicit-EXplicit (IMEX) Runge-Kutta (RK) schemes. More precisely, we use the implicit solver for the collision operator and the explicit one for all other terms. Generally the IMEX RK schemes can be defined by a double Butcher tableau

$$\begin{array}{c|c} \widetilde{c} & \widetilde{A} \\ \hline & \widetilde{w}^t \end{array} \qquad\qquad \begin{array}{c|c} c & A \\ \hline & w^t \end{array}$$

in which the two $\nu\times\nu$ matrices $\widetilde{A} = (\widetilde{a}_{ij})$ and $A = (a_{ij})$ are, respectively, the matrix for the explicit ($\widetilde{a}_{ij} = 0$ for $j \geq i$) and for the implicit discretizations; since, for efficiency, we consider only Diagonally Implicit RK (DIRK) schemes we have $a_{ij} = 0$, for $j > i$. Finally, coefficients $\widetilde{c}$ and c and vectors $\widetilde{w} = (\widetilde{w}_1, .., \widetilde{w}_\nu)^t$, $w = (w_1, .., w_\nu)^t$ are chosen to satisft the order conditions for the global scheme. We refer to [3, 9, 23, 37] for more details on IMEX schemes.

Here we only recall that, in order to guarantee that the AP and the AA properties are satisfied a sufficient condition is that the schemes are *globally stiffly accurate* (GSA). An IMEX-RK method is called *implicitly stiffly accurate* if the corresponding DIRK method is *stiffly accurate*, namely

$$a_{\nu i} = w_i, \quad i = 1, \ldots, \nu.$$

If, in addition, the explicit method satisfies

$$\widetilde{a}_{\nu i} = \widetilde{w}_i, \quad i = 1, \ldots, \nu,$$

then it is said to be *globally stiffly accurate* or simply *stiffly accurate*. The GSA IMEX scheme we use is a global second order method, which has 2 stages for explicit term and 4 stages for the implicit one. The corresponding matrix coefficients are

$$\begin{array}{c|cccc} 0 & 0 & 0 & 0 & 0 \\ 0 & 0 & 0 & 0 & 0 \\ 1 & 0 & 1 & 0 & 0 \\ 1 & 0 & 1/2 & 1/2 & 0 \\ \hline & 0 & 1/2 & 1/2 & 0 \end{array} \qquad \begin{array}{c|cccc} \delta & \delta & 0 & 0 & 0 \\ 0 & -\delta & \delta & 0 & 0 \\ 1 & 0 & 1-\delta & \delta & 0 \\ 1 & 0 & 1/2 & 1/2-\delta & \delta \\ \hline & 0 & 1/2 & 1/2-\delta & \delta \end{array}$$

which depends on δ. Choosing $\delta = 2$ one obtains monotonicity ([18]).

At time $t^n = n\Delta t$, the IMEX-RK scheme applied to equation (13) reads for the stages $F_{k,K} = (F^{(l)}_{k,K})_l$, $l = 1, \ldots, \nu$, of the kinetic variable $f_{k,K}$

$$\begin{aligned} F_{k,K} = f^n_{k,K}\overline{e} - \Delta t\widetilde{A}\left(h^n v_k \cdot \nabla_x F_{k,K} + h^n v_k \cdot \nabla_x \overline{\mathcal{M}}_k[\boldsymbol{P}_H] + \overline{E} \cdot \nabla_v F_{k,K}\right) \\ + \widetilde{A}F_k\left(h^{n+1} - h^n\right) + \Delta t\ A\ \frac{1}{\overline{\varepsilon}}\left(h^{n+1}\overline{\mathcal{M}}_k[\boldsymbol{P}] - F_{k,K}\right) \end{aligned} \tag{14}$$

while for the numerical solution we have

$$\begin{aligned} f_{k,K}^{n+1} = f_{k,K}^{n} - \Delta t \widetilde{w}^t \left(h^n v_k \cdot \nabla_x F_{k,K} + h^n v_k \cdot \nabla_x \overline{\mathcal{M}}_k[\boldsymbol{P}_H]) + \overline{E} \cdot \nabla_v F_{k,K} \right) \\ + \widetilde{w}^t F_k (h^{n+1} - h^n) + \Delta t \; w^t \; \frac{1}{\overline{\varepsilon}} \left(h^{n+1} \overline{\mathcal{M}}_k[\boldsymbol{P}] - F_K \right). \end{aligned} \tag{15}$$

We denoted by $\overline{e} = (1, \dots, 1) \in \mathbb{R}^\nu$, by $F_k = (F_k^{(l)})_l$, $l = 1, \dots, \nu$ the stage values for the global function f_k^n, by $\boldsymbol{P}$ the matrix corresponding to the stage values of the moments $\boldsymbol{\varrho}^n = (\rho^n, \rho^n u^n, \mathcal{E}^n)^t$, then by $\overline{\mathcal{M}}_k = (\mathcal{M}_k[\boldsymbol{P}^{(l)}])_l$ the stages of the discretized maxwellian, by $\overline{E} = (E^{(l)})_l$ those for the electric field E^n and by $\overline{\varepsilon} = (\varepsilon^{(l)})_l$ those for ε^n. Here and in the following, similar notations are used for kinetic and fluid variables. When occurring stages multiplications and divisions in vectors expressions are intended component by component.

Applying the same IMEX-RK scheme to system (11) gives for the stages $l = 1, \dots, \nu$ of the hydrodynamic system

$$\boldsymbol{P}_H = \boldsymbol{r}_H^n \overline{e} - \Delta t \, (1 - h^n) \widetilde{A} \Big(\nabla_x \cdot \mathcal{T}_H + \Delta v \sum_k \boldsymbol{m}_k v_k \cdot \nabla_x F_{k,K} \Big) + \Delta t \widetilde{A} \mathcal{S}_H \overline{E} - \widetilde{A} \boldsymbol{P} (h^{n+1} - h^n) \tag{16}$$

while for the numerical solution we have

$$\boldsymbol{\varrho}_H^{n+1} = \boldsymbol{\varrho}_H^n - \Delta t \, (1 - h^n) \widetilde{w}^t \Big(\nabla_x \cdot \mathcal{T}_H + \Delta v \sum_k \boldsymbol{m}_k v_k \cdot \nabla_x F_{k,K} \Big) + \Delta t \, \widetilde{w} \, \mathcal{S}_H \overline{E} - \widetilde{w} \boldsymbol{P} (h_i^{n+1} - h_i^n), \tag{17}$$

where we defined by $\mathcal{T}_H = (\rho_H u_H, \rho_H u_H \otimes u_H + p_H I, (\mathcal{E}_H + p_H) u_H)^t$ the vector containing the stages fluxes and we set $\mathcal{S}_H = (0, \rho_H, \rho_H u_H)^t$. The electric field stages $\overline{E} = (E^{(l)})_l$ are computed at each stage by solving the corresponding Poisson equation. Observe that the application of the IMEX strategy to the hydrodynamics system (11) reduces to a full explicit scheme.

In the above discretization, we assume the coupling function at time $n+1$ is a function of the moments at time n, i.e. $h^{n+1} = h(\boldsymbol{\varrho}^n)$, since we need to know which kind of description to use at any location of the domain to advance in time while we want to avoid introducing implicitness if not strictly necessary. Assume now h^{n+1} known, the details of this computation will be given in the next section. Then $\boldsymbol{\varrho}_H^{n+1}$ can be computed thanks to formulas (16) and (17) being all the terms in the equation explicit. Instead for the kinetic distribution f_K^{n+1} in the formulas (14) and (15) we need to implicitly evaluate the collision operator. In order to do that we need to compute the macroscopic moments $\boldsymbol{\varrho} = \boldsymbol{\varrho}_H + \boldsymbol{\varrho}_K$ and their stages $\boldsymbol{P}$ which then will uniquely define the Maxwellian state. To do so, we apply the same IMEX scheme described above, in practice only the explicit part, to the equation for the complete macroscopic moments to get for the stage values

$$\boldsymbol{P} = \boldsymbol{\varrho}^n \overline{e} - \Delta t \, \widetilde{A} \int \boldsymbol{m} \Big(v \cdot \nabla_x F + E \cdot \nabla_v F \Big) \, dv \, . \tag{18}$$

where $F = F_K + \overline{\mathcal{M}}[\boldsymbol{P}_H]$. Observe that this does not substantially increase the computational cost of the scheme since we need to compute the transport terms in the right hand side of equation (18) anyway to compute f_K^{n+1}. The only additional cost of the IMEX strategy, compared to a full explicit strategy, is due to the computation of the explicit term $E \cdot \nabla_v \mathcal{M}_k[\boldsymbol{P}_H]$, which is different from zero only inside buffers. Such cost is really a minor drawback compared to the gain we obtain thanks to the implicit computation of the collisions. Observe moreover that since we use only GSA IMEX schemes, the computation of the numerical solution is simply $f_K^{n+1} = F_K^{(\nu)}$, $\boldsymbol{\varrho}_H^{n+1} = P_H^{(\nu)}$ and $\boldsymbol{\varrho}^{n+1} = P^{(\nu)}$.

Thanks to the above discretization, the time step restriction for our coupled system reduces to only the classical hyperbolic CFL condition for systems of balance laws

$$\Delta t \, \frac{\max \{ \, |v_{min}|, |v_{max}|, 2\alpha \, \}}{\Delta x} \leq 1,$$

where α is the maximum of the eigenvalues of the hyperbolic system (11) and the multiplying factor 2 is due to the second order space discretization. For a general test case it would be necessary to consider also the (eventual) time step restriction due to the electric field. However, in the numerical tests we have considered it never becomes relevant and we omit this restriction here.

4.2.1 Splitting technique

The scheme proposed in the previous paragraph does not guarantee positivity of the distribution function f_K. Observe in fact that the term which models the time evolution of the different regions which is nothing else that the discrete time derivative of the cut-off function h in equations (14) and (15) does not depend on the time step Δt. This implies that there does not exist time step limitations that can be imposed which can guarantee the distribution function f_K to remain positive during the simulations.

However, in many applications positivity turns to be a very important property, this means that in the construction of the numerical scheme special care should be employed to permit preservation of positive states. In order to solve this problem we used a particular splitting technique, similar to that proposed in [13] for gas dynamics models. In practice, it is a splitting between the time integration of the physical variables and that of the coupling function h. Only for the sake of simplicity we show here how to write this splitting for a first order method. The generalization to higher order time discretization is straightforward.

In the first step of the splitting we approximate the equations $\partial_t f_K = \partial_t h f_K$ and $\partial_t \varrho_H = -\partial_t h \varrho_H$ by

$$\begin{aligned} f_K^* &= h^{n+1}\, f^n \\ \boldsymbol{\varrho}_H^* &= (1 - h^{n+1})\, \boldsymbol{\varrho}^n. \end{aligned} \tag{19}$$

In the second step we solve the rest of the coupled model with initial data f_K^* and ϱ_H^*

$$\begin{aligned} f_K^{n+1} = f_K^* &- \Delta t\, h^{n+1}\Big(v_k \cdot \nabla_x f_K^* + v_k \cdot \nabla_x \mathcal{M}[\boldsymbol{\varrho}_H^*]\Big) - \Delta t\, E \cdot \nabla_v f_K^* \\ &+ \frac{\Delta t}{\varepsilon^{n+1}} \left(h^{n+1} \mathcal{M}[\boldsymbol{\varrho}^{n+1}] - f_K^{n+1}\right) \end{aligned} \tag{20}$$

$$\boldsymbol{\varrho}_H^{n+1} = \boldsymbol{\varrho}_H^* - \Delta t\, (1 - h^{n+1}) \Big(\nabla_x \cdot \mathcal{T}_H^* + \Delta v \sum_k \boldsymbol{m}_k v_k \cdot \nabla_v f_{k,K}^*\Big) + \Delta t\, E\, \mathcal{S}_H^*. \tag{21}$$

Observe now that the first step of the splitting (19) is positive for construction if the distribution f_K and the density and energy of the hydrodynamic part ϱ_H are positive at time n. The second step of the splitting procedure (20-21) can be made positive with a limitation of the time step Δt which will depend on the space discretization choices. We conclude this part observing that this time step limitations which guarantee positivity will be now the classical ones used for guarantee positivity of conservation laws and kinetic equations. As an example if also a first order upwind space discretization is chosen for discretizing the transport part of the kinetic equation (20), positivity is guarantee if $(1 - \frac{\Delta t v}{\Delta x} - \frac{\Delta t E}{\Delta v}) \geq 0$.

For higher order time discretizations, at the beginning of each time step we perform step one and then compute starred kinetic stage values F_K^* iteratively using f_K^* and applying the IMEX strategy as in (20) and (21). The same holds for the hydrodynamic moments.

4.3 Space discretization

In this paragraph we describe the space discretization and we finally derive the fully discretized scheme for the coupled system (11-12). We introduce a spatial Cartesian uniform grid defined by a multi-index $\mathcal{I}$ of $\mathbb{N}^d$, defined by $\mathcal{I} = \left\{i = (i^j)_{j=1}^d,\ 0 \leq i^j \leq N_x^j\right\}$, where $\{N_x^j\}$ are some given bounds. We also set the grid $\mathcal{X} = \{x_i = a_x + i\Delta x,\ i \in \mathcal{I}\}$ in $\mathbb{R}^d$, where $a_x \in \mathbb{R}^d$ is an arbitrary vector and Δx is a scalar which represents the grid step in the physical space. In formulas below, given a generic grid function $(g_{k,i})$,

we denote by $\Gamma_{k,i}(g)$ a second order numerical discretization of $v_k \cdot \nabla_x g_{k,i}$ and by $\gamma_{k,i}(g)$ a second order numerical discretization of $\overline{E}_i \cdot \nabla_v g_{k,i}$. The former is defined as

$$\Gamma_{k,i}(g) = \frac{1}{\Delta x}\left(\varphi_{k,i+\frac{1}{2}} - \varphi_{k,i-\frac{1}{2}}\right),$$

where

$$\varphi_{k,i+\frac{1}{2}}(g) = \frac{1}{2}\big(G_{k,i} + G_{k,i+1}\big) - \frac{1}{2}v_k\big(g_{k,i+1} - g_{k,i}\big) + \frac{1}{4}\big(\sigma_i^+ - \sigma_{i+1}^-\big)$$

and

$$\sigma_i^{\pm} = \left(G_{k,i+1} \pm v_k g_{k,i+1} - G_{k,i} \mp v_k g_{k,i}\right)\Phi(\chi_i^{\pm})$$

with Φ the Van Leer slope limiter, $\chi^{\pm}$ the ratio of consecutive discrete gradients of the function $g_{k,i}$, $G = vg$ (see the reference papers and book [24, 25, 33] for details). The numerical flux $\gamma_{k,i}(g)$ can be computed in the same way as $\Gamma_{k,i}(g)$ simply replacing the space with the velocity variable. If no discontinuities arise along the velocity variable (which is often the case), the simpler less costly second order central finite difference discretization could also be used for $\nabla_v g_{k,i}$.

With these notations, the fully discretized scheme for equation (12) becomes as follows: perform step one of the splitting as in (19) and then, for each $i \in \mathcal{I}$ and for each $k \in \mathcal{V}$ compute for the stages $l = 1, \dots, \nu$

$$\begin{aligned} F_K^* = f_{k,i,K}^* \overline{e} - \Delta t \widetilde{A}\left(h_i^{n+1}\Gamma_{k,i}(F_K^* + \overline{\mathcal{M}}[\boldsymbol{P}_H^*]) + \gamma_{k,i}(F_K^*)\right) \\ + \Delta t\ A\ \frac{1}{\overline{\varepsilon}^*}\left(h_i^{n+1}\overline{\mathcal{M}}[\boldsymbol{P}^*] - F_K^*\right) \end{aligned} \tag{22}$$

and $f_{k,i,K}^{n+1} = F_K^{(\nu),*}$ for the numerical solution.

Concerning the hydrodynamic system, we distinguish two cases: buffer ($0 < h < 1$) and hydrodynamic ($h = 0$) regions. Inside buffer regions, in order to discretize system (11), we integrate over the velocity space the numerical fluxes $\Gamma_{k,i}$. This gives for the stages, for each $i \in \mathcal{I}$

$$\boldsymbol{P}_H^* = \boldsymbol{\varrho}_{i,H}^* \overline{e} - \Delta t\ \widetilde{A}\ \Delta v \sum_k \boldsymbol{m}_k\Big((1 - h_i^{n+1})\ \Gamma_{k,i}(\mathcal{M}[\boldsymbol{\varrho}_H^*] + F_K^*) + \gamma_{k,i}([\boldsymbol{\varrho}_H^*])\Big) \tag{23}$$

while for the numerical solution we simply have $\boldsymbol{\varrho}_{i,H}^{n+1} = \boldsymbol{P}_H^{(\nu),*}$. This has been done in order to ensure global conservation properties to our scheme. Observe in fact that if we used two conservative but different discretizations for the kinetic distribution f_K and for the hydrodynamic moments $\boldsymbol{\varrho}_H$, this would not guarantee that the total distribution $f = f_K + M[\boldsymbol{\varrho}_H]$ is discretized by a conservative method. The computational cost of the proposed method inside buffer regions is thus comparable to the one needed to solve the kinetic equation. On the other hand inside hydrodynamic regions, being $f_K = 0$ and $f = M[\boldsymbol{\varrho}_H]$, any conservative numerical scheme can be used to solve the moment equations (11). We then choose the following scheme for each $i \in \mathcal{I}$ for the stages

$$\boldsymbol{P}_H^* = \boldsymbol{\varrho}_{i,H}^* - \Delta t\ (1 - h_i^{n+1})\ \widetilde{A}\ \Gamma_i(\mathcal{T}_H^*) + \Delta t\ \widetilde{A}\ \mathcal{S}_H^*\ \overline{E}_i \tag{24}$$

and for the numerical solution we still have $\boldsymbol{\varrho}_{i,H}^{n+1} = \boldsymbol{P}_H^{(\nu),*}$. This means we choose the same numerical fluxes as before (actually their non linear version) but now we apply them directly to the macroscopic variables instead of applying them to the kinetic ones (i.e. to F_K^* and $\overline{\mathcal{M}}[\boldsymbol{P}_H^*]$ and then summing to estimate the integrals). The discrete flux $\Gamma_i(g)$ is defined as $\Gamma_{k,i}$ but for a one dimensional function and with $v_k = 1$. The computational cost of the coupling method is thus strongly reduced.

4.4 Memory saving implementation

In many industrial and practical applications, requirements in terms of memory space may become huge and in some cases they could also prevent the possibility of performing realistic multidimensional simulations. It is thus crucial to define numerical schemes that are efficient also in terms of total storage requests.

Domain decomposition techniques are especially designed to solve (in part at least) this kind of problem and they become more and more efficient as kinetic regions become smaller if compared to the unsustainable fully microscopic descriptions. Indeed, thanks to the decomposition of the domain it is possible to use only the strictly necessary amount of memory space related to variables f_K and $\boldsymbol{\varrho}_H$. That is, we allocate only the strictly necessary quantity of memory which is needed to store them in regions of the domain where they are defined and different from zero. Of course, this strategy becomes really efficient when kinetic areas are small compared to the whole domain since the microscopic description is the one that could cause memory overloading.

From the practical point of view at each time step, depending on the shape of the coupling function h^{n+1}, we have to allocate a sufficient memory quantity for the storage of f_K^{n+1}, i.e. all points in space where $h^{n+1} > 0$ (multiplied by the velocity grid), and similarly for $\boldsymbol{\varrho}_H^{n+1}$, i.e. all points in space where $h^{n+1} < 1$.

To this aim, it is possible to exploit memory management functions and libraries which are available in any modern high level programming language. At each time step we first compute h^{n+1}, then we perform memory allocations for all variables and then proceed with the time integration.

5 Breakdown criteria and dynamic decomposition

In this section we describe the time evolution of the coupling function h. Shocks, contact discontinuities, rarefaction waves and electric fields effects may cause local discontinuities or sharp gradients and all these components may actually move in time. It is thus crucial to move kinetic and buffer regions accordingly and simultaneously with these waves in order to represent the solution at any time and any location in space using the appropriate model. Our aim is to achieve computational speedup using, when possible, narrow kinetic areas and defining them only where it is strictly required.

The study of general breakdown criteria for fluid and plasmas is still a very active research field. We quote the works of [31] and [40] and the references therein for more detailed discussions on this subject. Here we only describe a few of them and concentrate on those we used. Some breakdown criteria can be deduced from both macroscopic and microscopic models while others are available only where the kinetic description is available. In the next two subsections we describe our choices and the corresponding strategies for their application.

5.1 Microscopic criteria

In regions where the kinetic or the coupled kinetic/fluid models are solved, we can exploit the knowledge of the full distribution function to measure the quantity of plasma particles which are not distributed according to the equilibrium. We can as well measure the fractions of momentum, energy and heat fluxes due to the non-equilibrium components. In more details, in every cell where $h > 0$ we measure

$$\lambda_1 = \int \Big| f_K - hM[\boldsymbol{\varrho}] \Big| dv, \qquad \lambda_2 = \int v \Big| f_K - hM[\boldsymbol{\varrho}] \Big| dv,$$
$$\lambda_3 = \int \frac{|v|^2}{2} \Big| f_K - hM[\boldsymbol{\varrho}] \Big| dv, \qquad \lambda_4 = \Big| \int v \frac{|v|^2}{2} (f_K - hM[\boldsymbol{\varrho}]) dv \Big|.$$

The breakdown of the kinetic/fluid model can be then measured by the following parameters

$$\beta_1 = \frac{\lambda_1}{\varrho},\ \beta_2 = \frac{\lambda_2}{\varrho\, u},\ \beta_3 = \frac{\lambda_3}{\mathcal{E}},$$

which measure the fraction of macroscopic quantities which are not in thermodynamical equilibrium. Another indicator is given by the heat flux, either in its absolute value ($\beta_4 = \lambda_4$) or with respect to the value of the equilibrium energy flux

$$\beta_4 = \frac{\lambda_4}{|\langle v\frac{1}{2}|v|^2 hM[\boldsymbol{\varrho}]\rangle|}.$$

In order to define a unique variable which tells us when to switch from one model to the other and which is available in every regime and in every region in space, we choose β_4 as the breakdown parameter. Indeed, as shown below, this is the only quantity which is possible to estimate also in fluid regions.

5.2 Macroscopic criteria

The criterion we propose is based on the asymptotic expansion of the distribution function with respect to ε. Indeed, when the Knudsen number ε is close to but not exactly zero, a better description of the dynamics of the particles is given by a Navier-Stokes-like system similar to (7) and not by an Euler-like one of type (6). When the two systems produce very close solutions, it means that the Euler-like model accurately represents the dynamics up to an acceptable accuracy. If, instead, the correction terms of the Navier-Stokes-like model with respect to the Euler-like system are large, it means that our fluid approximation is not sufficiently accurate and we need to switch to the kinetic description.

We proceed as follows: *a*) we estimate correction terms moduli at each grid point, *b*) if their values are larger then a fixed threshold we switch to the kinetic solver, *c*) otherwise we keep using the hydrodynamic description. Buffer zones are defined completely inside the macroscopic regions to be sure that the correct dynamics is computed. In formulas we have $\beta_4 = \lambda_4$, where now λ_4 is estimated thanks to the Hilbert expansion as

$$\lambda_4 = (\varepsilon\sigma u + q) \tag{25}$$

and it is nothing else than the heat flux of the Navier-Stokes equations. We now summarize the kinetic/fluid coupling function update algorithm.

We choose two threshold values $0 \leq \beta_{kin}, \beta_{NS} \leq 1$. The former defines the maximum errors we accept when using the fluid model instead of the kinetic one and the latter defines the tolerance for switching to the hydrodynamic model. In all areas of Ω in which $\beta_4 > \beta_{kin}$ it is necessary to define a new kinetic region; there we set $h = 1$ and then we define buffers to connect the new kinetic regions with the hydrodynamic ones. On the other hand, if $\beta_4 < \beta_{NS}$ then we can switch to the fluid description and thus define new macroscopic regions. At these points we set $h = 0$ and then we define buffers to connect with kinetic regions. When updating the coupling function, it is necessary to verify if buffers overlap or intersect in a wrong way and, if this is the case, they have to be changed. An easy solution is to eventually enlarge a little bit the kinetic area to ensure h has the desired shape.

5.3 Summary of the numerical scheme

We now resume the scheme proposed on the form of an algorithm.

Assume that $\boldsymbol{\varrho}_H^n, f_K^n, h^n, \phi^n$ are known in the whole phase space domain at time t_n and that the two threshold β_{kin} and β_{NS} have been fixed. Then we

1. compute the equilibrium parameter β_4 through (25);
2. if $\beta_4(x) > \beta_{kin}$ then set $h^{n+1}(x) = 1$ while if $\beta_4(x) < \beta_{NS}$ then set $h^{n+1}(x) = 0$;
3. define buffers between the new kinetic and fluid regions and, if any, merge overlapping buffers;

4. allocate the necessary memory for the storage of the kinetic and hydrodynamic variables;
5. advance the hydrodynamics moments $\boldsymbol{\varrho}_H^{n+1}$ in time using the splitting technique, i.e. using scheme (23) inside buffers and scheme (24) for the fully hydrodynamic regions;
6. compute, only where $h^{n+1} > 0$, the stages for the global moments $\boldsymbol{P}^*$ through (18) using the splitting technique. Then use $\boldsymbol{P}^*$ to compute $\overline{\mathcal{M}}^{n+1}[\boldsymbol{P}^*]$ and $\bar{\varepsilon}^*$;
7. advance the kinetic equation in time by using (22) and obtain f_K^{n+1};
8. update function f and its moments at time $n+1$;
9. update the electric potential ϕ^{n+1} using standard discretization for the Poisson equation.

6 Numerical tests

In this section we present several one dimensional numerical tests showing the capability of the presented method to accurately and efficiently describe multiscale plasma problems. In order to obtain the correct equation of state, we use a one-dimensional velocity space model which is able to account for three-dimensional velocity effects (see for example [14]). It is obtained from the full three-dimensional Vlasov-BGK equation using a reduction technique [26]. Considering, for instance, ions equation such model reads

$$\partial_t F + v \cdot \partial_x F + E \cdot \partial_v F = \frac{1}{\varepsilon}(M_F - F)$$
$$\partial_t G + v \cdot \partial_x G + E \cdot \partial_v G = \frac{1}{\varepsilon}(TM_F - G)$$

while the fluid energy is given by

$$\mathcal{E} = \sum_k \frac{1}{2} v_k^2 F_k + G_k.$$

In this way, it is possible to recover the correct hydrodynamic limit given by the standard Euler-type system even with a lower dimensional velocity space.

The thickness of the buffer zones is kept fixed and equal to $4\Delta x$ while the thickness of the kinetic and fluid regions vary according to the previously described criteria and can also shrink to zero. We use a moments dependent formula for the Knudsen number, i.e. $\varepsilon = \varepsilon_0/\rho$, with ε_0 a fixed constant. The value of this constant and the treatment of the boundary conditions are detailed for each test in the corresponding subsection.

6.1 One species plasma

Test 1: plasma expansion in a rarefied regime
In this first test we model a one dimensional plasma expansion into nearly vacuum. We consider a plasma constituted by one species of ions and a fixed background of electrons with the electric field self-consistently computed through the Poisson equation. This simulation mimics, for instance, the behavior of a plasma propulsor, like for example a plasma thruster.

At the beginning the distribution is in thermodynamical equilibrium everywhere and we impose a constant in time injection of equilibrium particles at the left corner of the domain. Observe that thanks to the use of GSA IMEX schemes we could also set the value of the mass density to zero inside the domain at the initial time, thus simulating an expansion occurring into vacuum

The velocity domain is $[-8, 8]$, the space domain is $x \in [x_L = 0, x_R = 1]$ and the plasma injection is fixed at x_L. We impose Dirichlet boundary conditions at the left corner (constant maxwellian injection) and Neumann boundary conditions at the right corner of the domain. We take 100 cells in physical space and 100 cells in velocity space. Initial conditions are such that on the left boundary the mass density is $\rho_L = 1$, the mean velocity is $u_L = 1$ and the temperature is $T_L = 1$ while all over the rest of the domain we set $\rho_R = 0.1$, mean velocity $u_R = 0$ and temperature $T_R = 0.5$. The value of ε_0 is set to $\varepsilon_0 = 0.001$. The cut-off function h is initialized as $h = 0$ everywhere. For the computation of the electric field we fix the values of the electric potential V at the extreme points of the domain, $V(x_L) = 0.1$ and $V(x_R) = 0$, the constant background density of electrons is $\rho_e = \rho_R$ and the Debye length is $\lambda^2 = 1$. Thresholds for the determination of the coupling function are $\beta_{kin} = 0.98$ and $\beta_{NS} = 10^{-2}$.

When the simulation starts at time $t_0 = 0$ the plasma starts to expand, a discontinuity arises and propagates from left to right. Meanwhile, the coupling function follows the evolution of the plasma and it identifies the breakdown of the fluid model. Correspondingly, the hydrodynamic area shrinks and the kinetic one starts to form. We show the mass, the velocity and the temperature densities of the ions at three different times: at time $t_i = 0.05$ in figure 1, at time $t_m = 0.15$ in figure 2 and at final time $t_f = 0.3$ in figure 3.

We report these results using the coupling, the fully kinetic and the fully hydrodynamic solvers in order to compare them. We observe that solutions obtained with the coupled method perfectly fits those found using the fully kinetic formulation everywhere. On the other hand we observe that the hydrodynamic model fails in describing the correct solutions (as reference data we consider the ones obtained through the kinetic solver). From the plots it is also possible to observe the evolution of the buffer zone. In this test case, no new hydrodynamic areas are created since thermodynamical equilibrium is not restored once the shock travels along the domain.

Test 2: plasma expansion in a hydrodynamic regime

In this second test we model a plasma expansion in a more dense regime. The setting of the problem is the same as the first test and if not otherwise specified the numerical setting coincide. In particular, we change the value of the Knudsen number ε_0 which is now fixed to $\varepsilon_0 = 7 \cdot 10^{-5}$ in order to represent a more dense regime.

We impose Dirichlet boundary conditions at the left corner (constant maxwellian injection) and Neumann boundary conditions at the right corner of the domain. Initial conditions are such that on the left boundary the mass density is $\rho_L = 1$, the mean velocity is $u_L = 1$ and the temperature is $T_L = 1$ while all over the rest of the domain we set $\rho_R = 0.01$, mean velocity $u_R = 0$ and temperature $T_R = 0.6$. Data for the computation of the electric field and the thresholds for the coupling functions are set as in the previous test.

When the simulation begins at time $t_0 = 0$ the plasma starts to expand and the discontinuity propagates towards the right. In this case, unlike in the previous test, a new hydrodynamic region is automatically created starting from the left corner. This is due to the fact that thermodynamical equilibrium is reestablished, because of the strong collisions, after the transit of the shock wave. We can see from figures 4-6 that our scheme is able to correctly track the regions in which the fluid model breaks down. We are able to use the kinetic model only where it is really necessary and use the much less costly macroscopic description elsewhere.

We again report the distributions of mass, velocity and temperature at three different times: at time $t_i = 0.037$ in figure 4, at an intermediate time $t_m = 0.1$ in figure 5 and at final time $t_f = 0.2$ in figure 6. In all the figures we plot the results obtained using the coupling, the kinetic and the hydrodynamic solvers. We can see that the results obtained with the coupled method perfectly fits those computed using the kinetic formulation all along the physical domain. Moreover, we see that using the hydrodynamic solver in areas of the domain which are far from equilibrium produces results which are, as expected, not exact. Also here we can view from the figures how the coupling function h evolves in time.

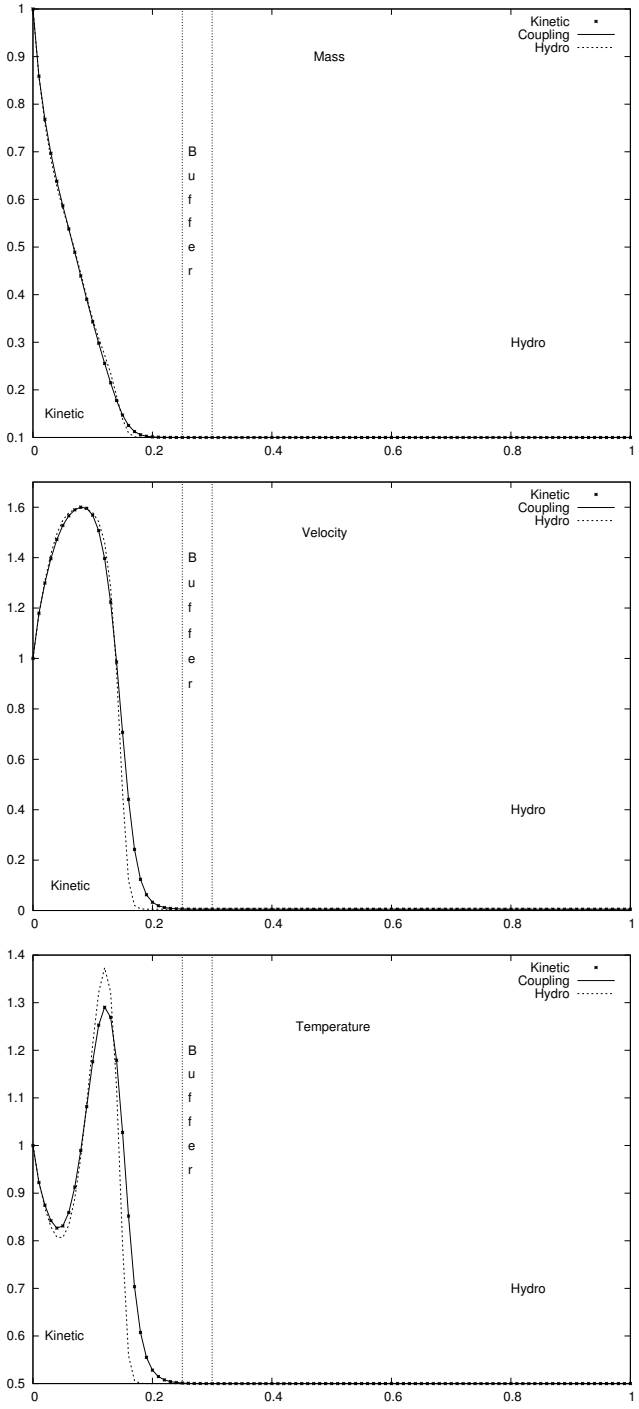

Figure 1: Test 1: mass (top), velocity (middle) and temperature (bottom). Results at time t_i obtained using the kinetic (dots), the coupled (line) and the hydrodynamic (dotted line) solvers.

6.2 Two species plasma

Test 3: plasma capacitor, cold ions
This test simulates the behavior of a two species plasma subject to electric field effects. The simulation is performed also in this case using a one dimensional setting for the space variable and the three dimensional one for velocity. We start with the plasma at equilibrium everywhere, with constant values of the macroscopic variables, and we assign a fixed potential difference at the edges of the domain which makes the system evolve. Even using only one dimension in space, this test shows the behavior of a condenser with a plasma located between its walls. This is true if, for instance, at least in some region inside the condenser the electric field (eventually) varies along the direction perpendicular to the walls but is constant along the direction parallel to the walls.

The velocity domain is $[-8, 8]$ and the space domain is $x \in [x_L = 0, x_R = 1]$. We impose Dirichlet boundary conditions (constant maxwellian injection) at both sides of the domain. We use 100 cells in physical space and 100 cells in velocity space. The cut-off function h is initialized as $h = 0$ everywhere. As initial conditions we start with kinetic variables at equilibrium and with constant moments values for both ions and electrons: we set mass density $\rho_i = 1$, mean velocity $u_i = 0$, temperature $T_i = 0.4$ and $\varepsilon_{0,i} = 10^{-5}$ and mass density $\rho_e = 0.1$, mean velocity $u_e = 0$, temperature $T_e = 0.4$ and $\varepsilon_{0,e} = 10^{-3}$. For the computation of the electric field we fix the values of the electric potential V at the extreme points of the domain, $V(x_L) = 2$ and $V(x_R) = 0$, the Debye length is $\lambda^2 = 1$ and $m_r = 5$. Thresholds for the determination of the coupling function are $\beta_{kin} = 1$ and $\beta_{NS} = 10^{-3}$.

When the potential difference is turned on at time $t_0 = 0$, the force applied by the electric field acts differently on ions and on electrons because of the difference between their masses and this difference breaks the symmetry of the system.

Moments distribution functions are represented at three different times to show their time evolution. In figures 7, 8 and 9 we compare mass, velocity and temperature distributions of both particles respectively at an initial time $t_i = 0.05$, at an intermediate time $t_m = 0.1$ and at the final time $t_f = 0.15$. In order to present more easy-to-read pictures, we omit the plot of the kinetic solution since it coincides with that obtained through the coupling method. The kinetic, hydrodynamic and buffer regions represented in these pictures are those only for electrons; we do not show those for ions in this case since they are, as desired, solved always using the macroscopic description and thus their coupling function is constantly equal to zero everywhere.

This tests shows that the two components of the plasma can be treated separately, each having its own independent domain decomposition coupling. In this case we reproduced the so called "cold ions" model, which means those where ions always remain in thermodynamical equilibrium and are always modeled by macroscopic equations.

Test 4: plasma capacitor, hot ions
In this last test we simulate the behavior of a two species plasma inside a capacitor in a more complex situation. The setting of the problem is similar to that of the previous one and we change some parameters in order to see the domain decomposition technique step-in also for the ions.

The values of the numerical setting constants which are not specified here coincide with those in Test 3. Also here we impose Dirichlet boundary conditions (constant maxwellian injection) at both sides of the domain. Concerning macroscopic moments this time we set mass density $\rho_i = 0.2$, mean velocity $u_i = 0$, temperature $T_i = 2$ and $\varepsilon_{0,i} = 10^{-3}$ and mass density $\rho_e = 0.1$, mean velocity $u_e = 0$, temperature $T_e = 2$ and $\varepsilon_{0,e} = 10^{-3}$. Values of the electric potential V at the extreme points of the domain are $V(x_L) = 5$ and $V(x_R) = 0$, the Debye length is $\lambda^2 = 1$ and $m_r = 2$.

In figures 10 and 11 we compare mass, velocity and temperature distributions of both particles respectively at an intermediate $t_m = 0.05$ and at the final time $t_f = 0.1$. We omit an initial step since distributions are still too close to see the difference and we again omit the plot of the kinetic solution

since it coincides with that obtained through the coupling method. In figure 12 we show the evolution of the two different coupling functions for ions and electrons at the same times at which we reported the snapshots for moments of the distribution functions.

7 Conclusion

In this paper we designed, described and tested a general approach which permits to simulate two species multiscale plasma models. This scheme can be extended without any difficulty to more than two species. We exploited the main benefits of both Automatic Domain Decomposition and Asymptotic Preserving time discretization techniques which permit to guarantee efficiency and precision for our approach. Moreover, we implemented and tested a memory saving strategy in order to make our scheme really efficient also regarding storage issues. The presented numerical tests, in one space dimension and three velocity dimensions, show we achieve the expected results.

Possible roads for future developments are simulations in two or three space dimensions and the design of a truly multiscale approach regarding (at least) the time variable. For truly real life application, a detailed study of the cost of the memory efficient implementation may also be interesting, i.e. verify when the application of such strategy really decreases the global (computational + memory) cost of the simulations and not only that regarding the storage.

References

[1] A. Alaia, G. Puppo, *A hybrid method for hydrodynamic-kinetic flow Part II Coupling of hydrodynamic and kinetic models* J. Comp. Phys., 231 (2012) pp. 5217–5242.

[2] O. Aktas, N.R. Aluru, *A combined continuum/DSMC technique for multiscale analysis of microfluidic filters*, J. Comp. Phys., 178 (2002) pp. 342–72.

[3] U. Ascher, S. Ruuth, R.J. Spiteri, *Implicit-explicit Runge-Kutta methods for time dependent Partial Differential Equations*, Appl. Numer. Math., 25 (1997) pp. 151–167.

[4] C. Bardos, F. Golse, D. Levermore, *Fluid dynamic limits of kinetic equations. I. Formal derivations*, J. Stat. Phys. 63 (1991) pp. 323–344.

[5] M. Bennoune, M. Lemou, L. Mieussens, *Uniformly stable numerical schemes for the Boltzmann equation preserving the compressible Navier-Stokes asymptotics*, J. Comp. Phys., 227 (2008) pp. 3781–3803.

[6] G. A. Bird, Molecular gas dynamics and direct simulation of gas flows, Clarendon Press, Oxford (1994).

[7] C.K. Birdsall, A.B. Langdon, Plasma Physics via Computer Simulations, Taylor and Fransis, (2004).

[8] J.F. Bourgat, P. LeTallec, B. Perthame, Y. Qiu, *Coupling Boltzmann and Euler equations without overlapping*, in Domain Decomposition Methods in Science and Engineering, AMS Contemp. Math., 157 (1994) pp. 377–398.

[9] M.H. Carpenter, C.A. Kennedy, *Additive Runge-Kutta schemes for convection-diffusion-reaction equations*, Appl. Numer. Math., 44 (2003) pp. 139–181.

[10] C. Cercignani, The Boltzmann equation and its applications, Springer-Verlag, New York, (1988).

[11] N. Crouseilles, P. Degond, M. Lemou, *A hybrid kinetic-fluid model for solving the gas dynamics Boltzmann BGK equation*, J. Comp. Phys., 199 (2004) pp. 776–808.

[12] P. Degond, F. Deluzet, L. Navoret, A.B. Sun, M.H. Vignal, *Asymptotic-Preserving Particle-In-Cell method for the Vlasov-Poisson system near quasineutrality*, J. Comp. Phys., 229 (2010) pp. 5630–5652.

[13] P. Degond, G. Dimarco, L. Mieussens, *A moving interface method for dynamic kinetic-fluid coupling*, J. Comp. Phys., 227 (2007) pp. 1176–1208.

[14] P. Degond, G. Dimarco, L. Mieussens, *A multiscale kinetic-fluid solver with dynamic localization of kinetic effects*, J. Comp. Phys., 229 (2010) pp. 4907–4933.

[15] P. Degond, S. Jin, L. Mieussens, *A Smooth Transition Between Kinetic and Hydrodynamic Equations* , J. Comp. Phys., 209 (2005) pp. 665–694.

[16] G. Dimarco, L. Mieussens, V. Rispoli, *A smooth transition approach between the Vlasov-Poisson and the Euler-Poisson system*, proceedings of the `DD21` conference. Springer, Lecture Notes in Computational Science and Engineering.

[17] G. Dimarco, L. Pareschi, *Hybrid multiscale methods II. Kinetic Equations*, SIAM J. Mult. Mode. Sim., 6 (2007) pp. 1169–1197.

[18] G. Dimarco, L. Pareschi, *Asymptotic preserving implicit-explicit Runge-Kutta methods for nonlinear kinetic equations*, C. R. Acad. Sci. Paris, Ser. I 350 (2012) pp. 481–486.

[19] G. Dimarco, L. Pareschi, *Exponential Runge-Kutta methods for stiff kinetic equations*, J. Numer. Anal., 49 (2011) pp. 2057–2077.

[20] G. Dimarco, L. Pareschi, V. Rispoli, *Implicit-Explicit Runge-Kutta schemes for the Boltzmann-Poisson equation for semiconductors*, Submitted.

[21] F. Filbet, S. Jin, *A class of asymptotic preserving schemes for kinetic equations and related problems with stiff sources*, J. Comp. Phys., 229 (2010) pp. 7625–7648.

[22] E. Gabetta, L. Pareschi, G. Toscani, *Relaxation schemes for nonlinear kinetic equations*, J. Numer. Anal., 34 (1997) pp. 2168–2194.

[23] E. Hairer, G. Wanner, *Solving Ordinary Differential Equations* II: Stiff and Differential-Algebraic Problems (1987) Springer-Verlag, New York.

[24] A. Harten, *High Resolution Schemes for Hyperbolic Conservation Laws*, J. Comp. Phys., 135 (1997) pp. 260–278.

[25] C. Hirsch, Numerical Computation of internal and external flows, vol. 2, John Wiley & Sons (1994).

[26] A.B. Huang, P.F. Hwang, *Test of statistical models for gases with and without internal energy states*, Phys. Fluids, 16 (1973) pp. 466–475.

[27] S. Jin, *Efficient Asymptotic-Preserving (AP) schemes for some multiscale kinetic equations*, J. Sci. Comp., 21 (1999) pp. 441–454.

[28] S. Jin, L. Pareschi, G. Toscani, *Uniformly accurate diffusive relaxation schemes for transport equations*, J. Numer. Anal., 38 (2000) pp. 913–936.

[29] A. Klar, *A numerical method for kinetic semiconductor equations in the drift diffusion limit*, J. Sci. Comp., 19 (1998) pp. 2032–2050.

[30] V.I. Kolobov, R.R. Arslanbekov,V.V. Aristov, A.A. Frolova, S.A. Zabelok, *Unified Solver for Rarefied and Continuum Flows with Adaptive Mesh and Algorithm Refinement*, J. Comp. Phys., Vol. 223 No. 2, pp. 589–608 (2007).

[31] V.I. Kolobov, R.R. Arslanbekov, V.V. Aristov, A.A. Frolova, S.A. Zabelok, *Towards adaptive kinetic-fluid simulations of weakly ionized plasmas*, J. Comp. Phys., 231 (2012) pp. 839–869.

[32] M. Lemou, L. Mieussens, *A New Asymptotic Preserving Scheme Based on Micro-Macro Formulation for Linear Kinetic Equations in the Diffusion Limit*, J. Sci. Comp., 31 (2008) pp. 334–368.

[33] R. J. LeVeque, Numerical methods for conservation laws, Lectures in Mathematics, ETH Zrich. Birkhuser (1990).

[34] D. Levermore, W.J. Morokoff, B.T. Nadiga, *Moment realizability and the validity of the Navier Stokes equations for rarefied gas dynamics*, Phys. Fluids, 10 (1998) pp. 3214–3226.

[35] L. Mieussens, *Discrete Velocity Model and Implicit Scheme for the BGK Equation of Rarefied Gas Dynamic*, Math. Models and Methods in Applied Sciences, 10 (2000) pp. 1121–1149.

[36] L. Mieussens, *Convergence of a discrete-velocity model for the Boltzmann-BGK equation*, Comp. Math. Appl., 41 (2001) pp. 83–96.

[37] L. Pareschi, G. Russo, *Implicit-Explicit Runge-Kutta methods and applications to hyperbolic systems with relaxation*, J. Sci. Comp., 25 (2005) pp. 129–155.

[38] S. Pieraccini, G. Puppo, *Implicit-Explicit schemes for BGK Kinetic Equations*, J. Sci. Comp., 32 (2007) pp. 1–28.

[39] T.E. Schwartzentruber, L.C. Scalabrin, I.D. Boyd, *A modular particle continuum numerical method for hypersonic non-equilibrium gas flows*, J. Comp. Phys., 225 (2007) pp. 1159–1174.

[40] Q. Sun, I.D. Boyd, G.V. Candler, *A hybrid continuum/particle approach for modeling subsonic, rarefied gas flows*, J. Comp. Phys., 194 (2004) pp. 256–277.

[41] S. Tiwari, *Coupling of the Boltzmann and Euler equations with automatic domain decomposition*, J. Comp. Phys., 144 (1998) pp. 710–726.

[42] S. Tiwari, A. Klar, *An adaptive domain decomposition procedure for Boltzmann and Euler equations*, J. Comp. Appl. Math., 90 (1998) pp. 223–37.

[43] W.L. Wang, I.D. Boyd, *Predicting Continuum breakdown in Hypersonic Viscous Flows*, Phys. Fluids, 15 (2003) pp. 91–100.

[44] H.S. Wijesinghe, N.G. Hadjiconstantinou, *Discussion of Hybrid Atomistic-Continuum Methods for Multiscale Hydrodynamics*, Int. J. Multi. Comp. Eng., 2 (2004) pp. 189–202.

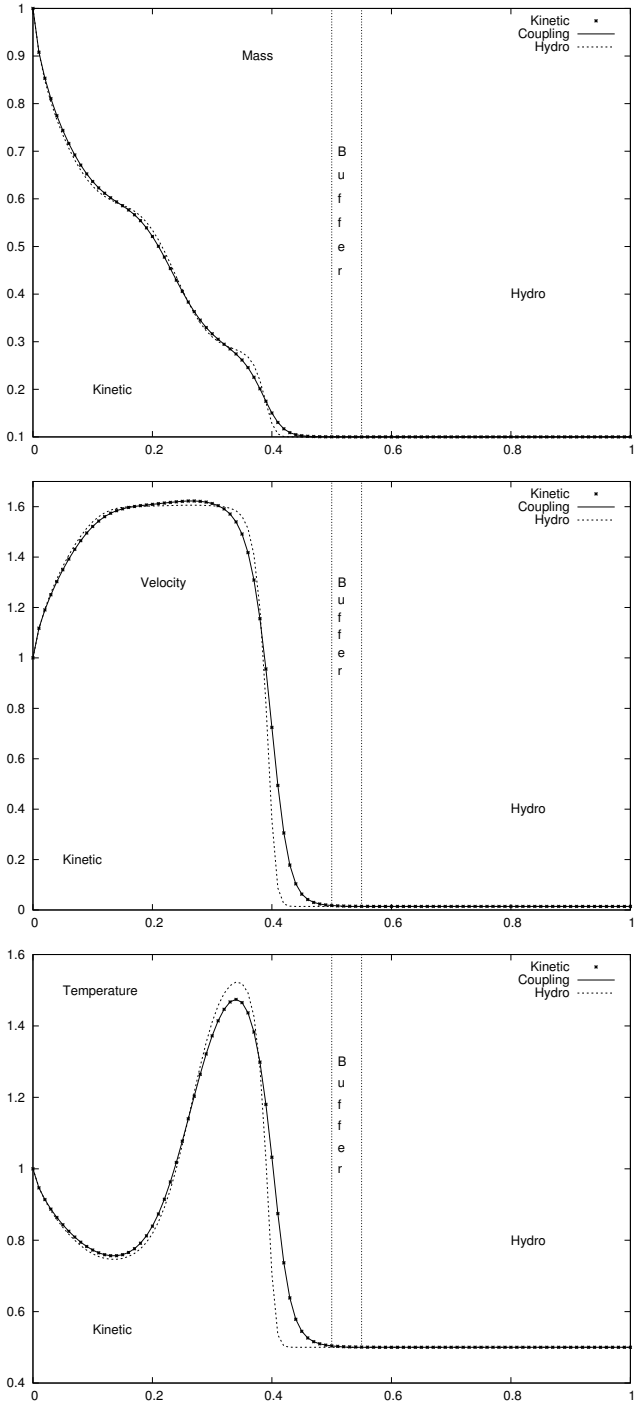

Figure 2: Test 1: mass (top), velocity (middle) and temperature (bottom). Results at time t_m obtained using the kinetic (dots), the coupled (line) and the hydrodynamic (dotted line) solvers.

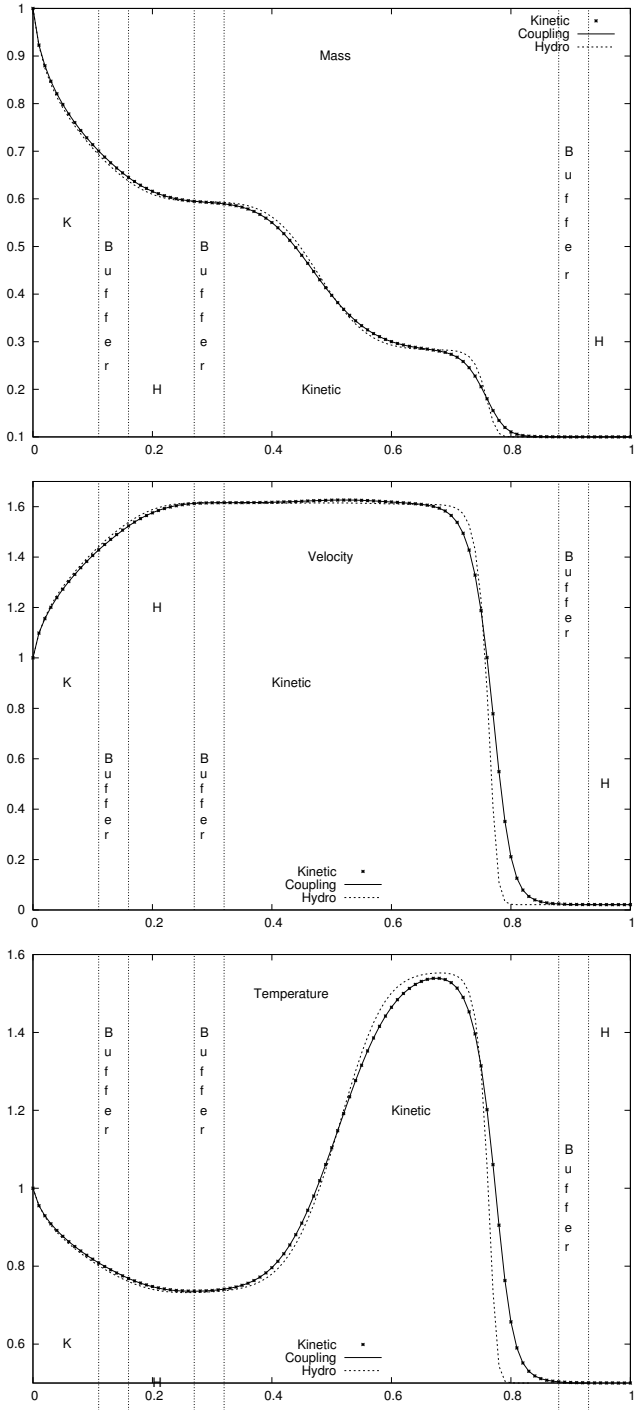

Figure 3: Test 1: mass (top), velocity (middle) and temperature (bottom). Results at time t_f obtained using the kinetic (dots), the coupled (line) and the hydrodynamic (dotted line) solvers.

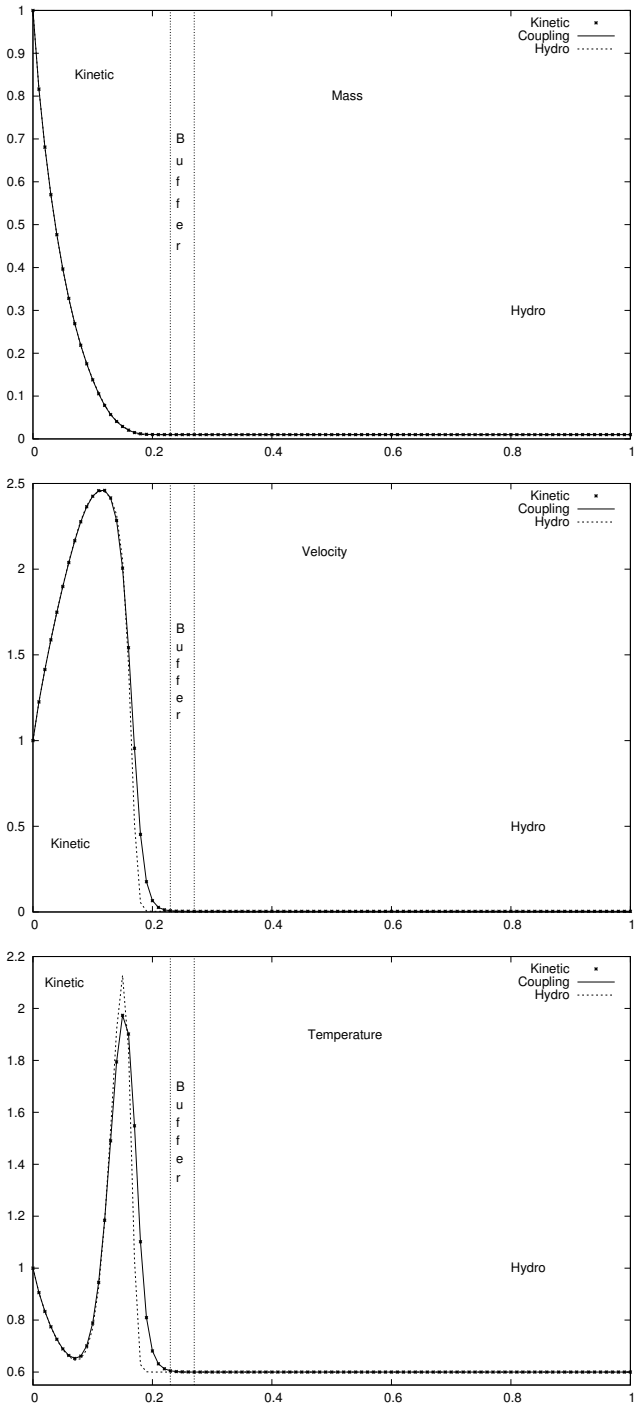

Figure 4: Test 2: mass (top), velocity (middle) and temperature (bottom). Results at time t_i obtained using the kinetic (dots), the coupled (line) and the hydrodynamic (dotted line) solvers.

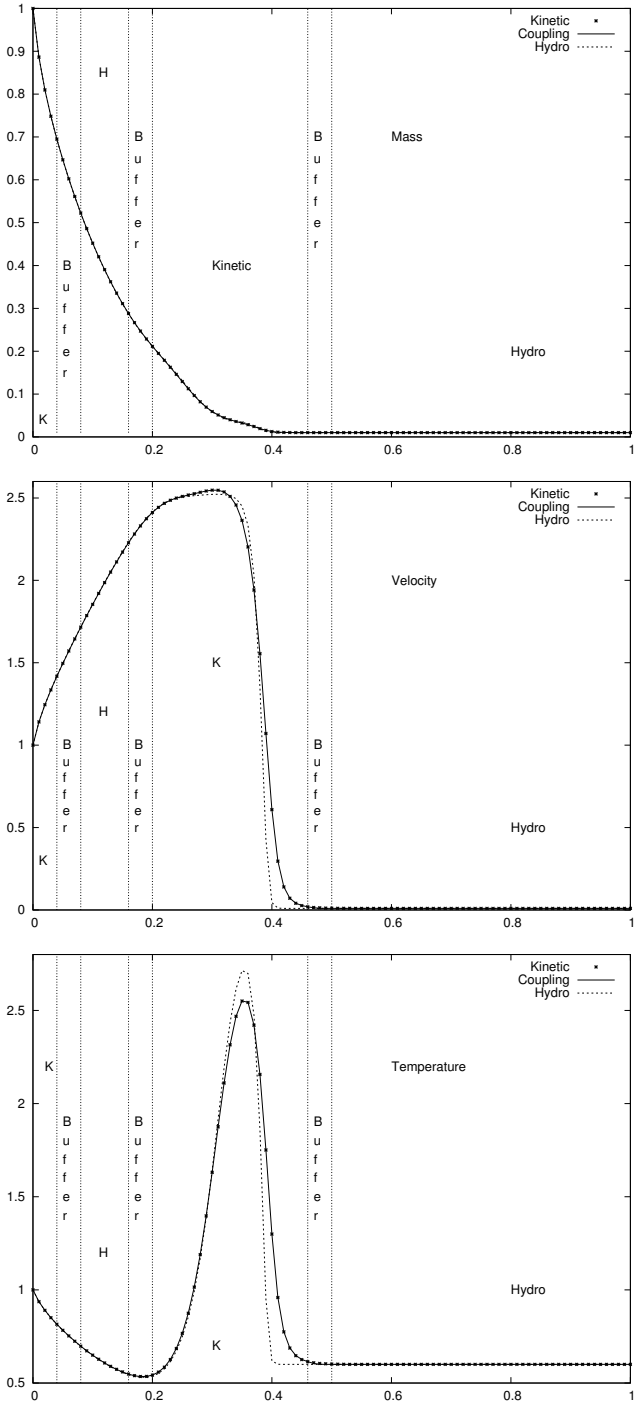

Figure 5: Test 2: mass (top), velocity (middle) and temperature (bottom). Results at time t_m obtained using the kinetic (dots), the coupled (line) and the hydrodynamic (dotted line) solvers.

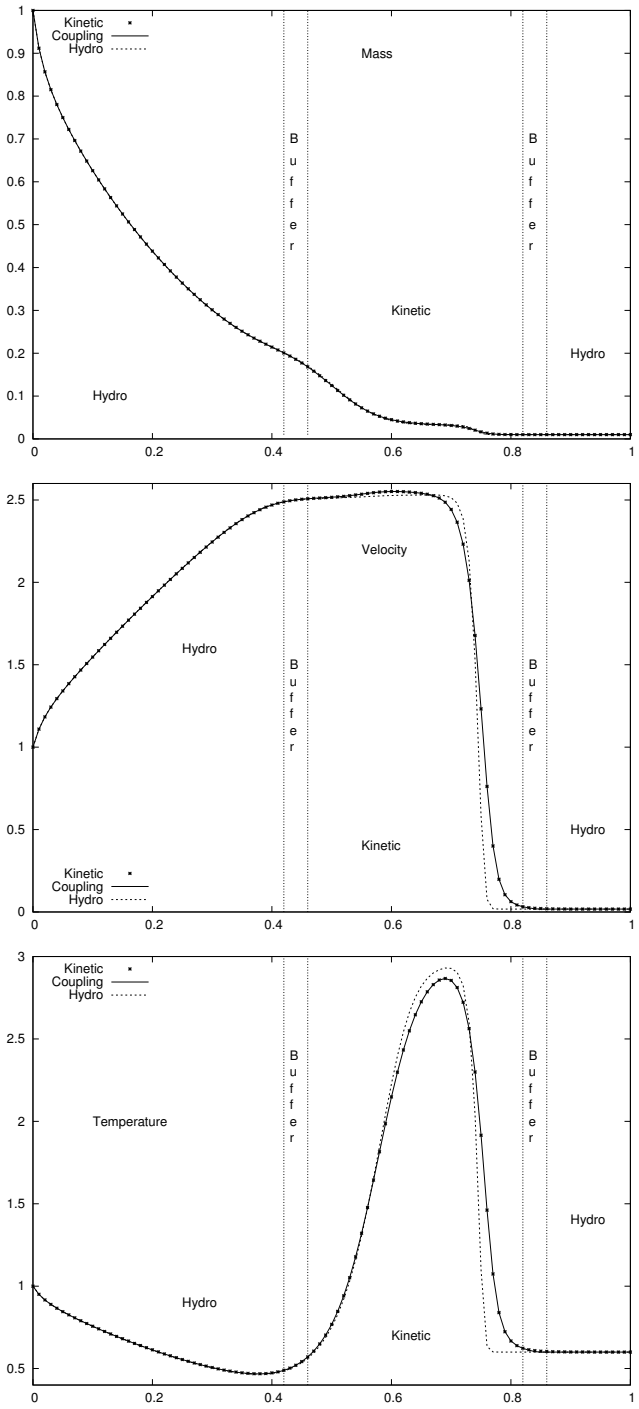

Figure 6: Test 2: mass (top), velocity (middle) and temperature (bottom). Results at time t_f obtained using the kinetic (dots), the coupled (line) and the hydrodynamic (dotted line) solvers.

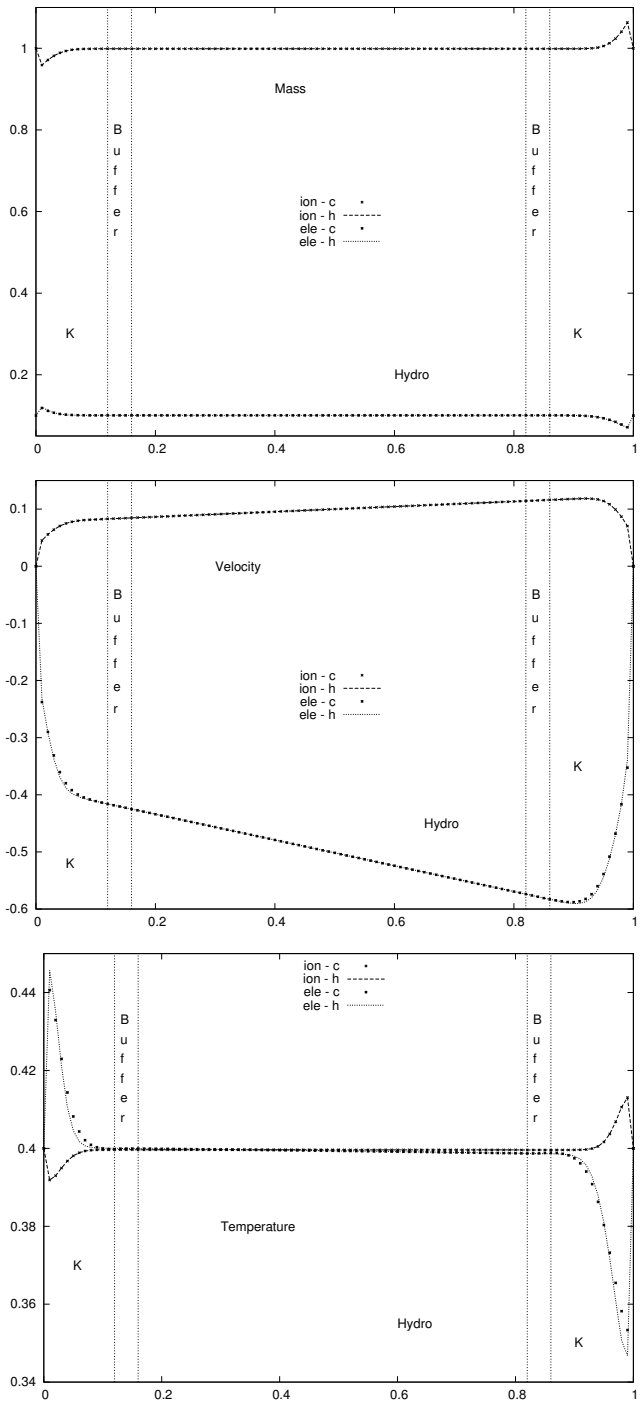

Figure 7: Test 3: mass (top), velocity (middle) and temperature (bottom). Results at time t_i using the the coupled ($\bullet$ for ions and $\times$ for electron) and the hydrodynamic (dashed line for ions and dotted line for electrons) solvers.

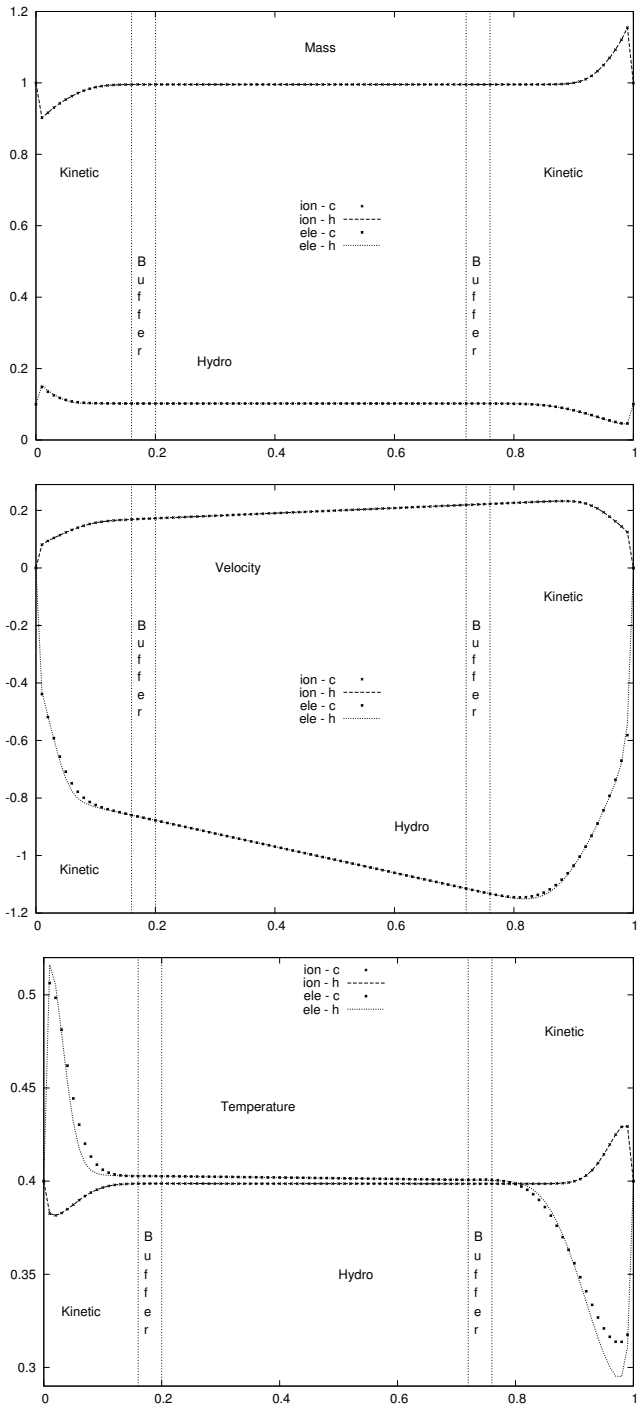

Figure 8: Test 3: mass (top), velocity (middle) and temperature (bottom). Results at time t_m using the the coupled ($\bullet$ for ions and $\times$ for electron) and the hydrodynamic (dashed line for ions and dotted line for electrons) solvers.

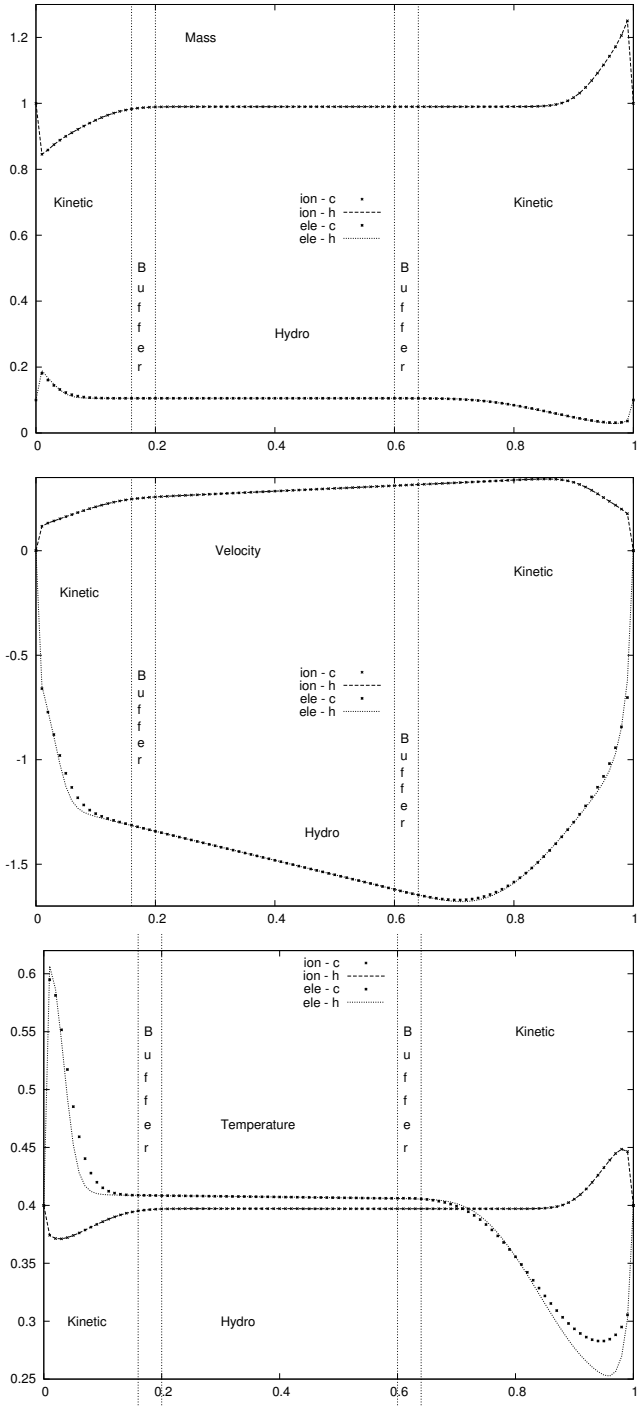

Figure 9: Test 3: mass (top), velocity (middle) and temperature (bottom). Results at time t_f using the the coupled ($\bullet$ for ions and $\times$ for electron) and the hydrodynamic (dashed line for ions and dotted line for electrons) solvers.

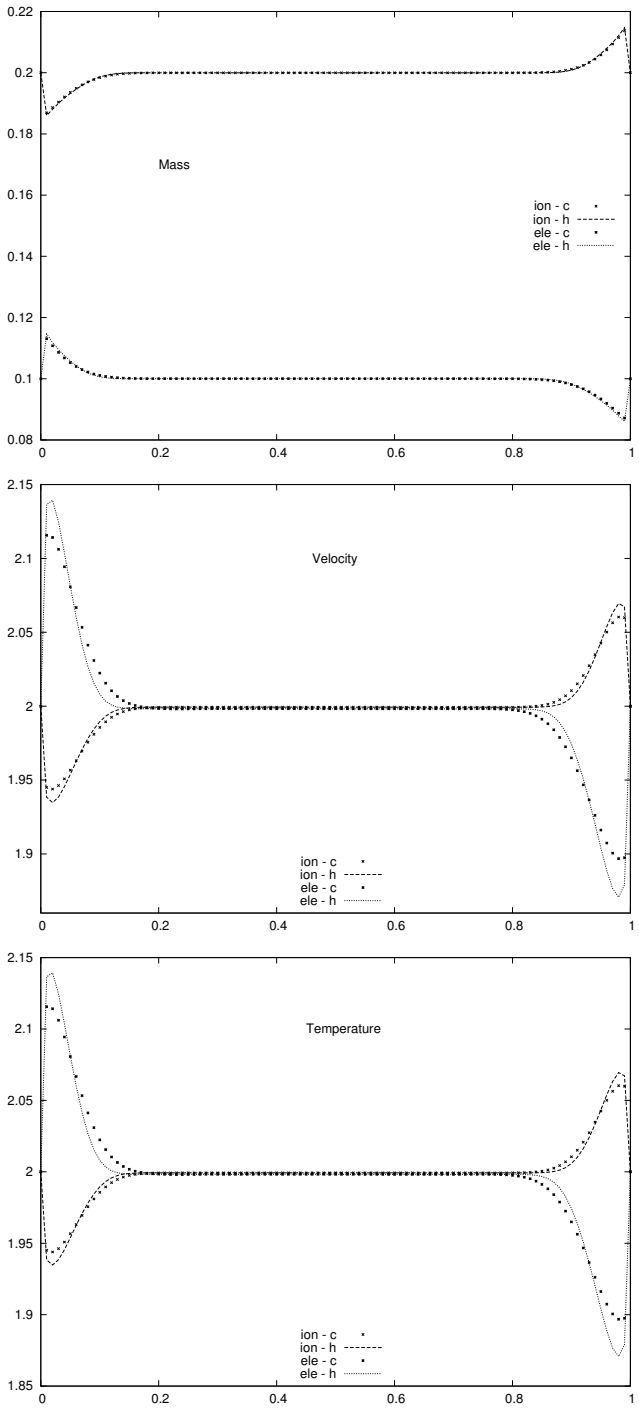

Figure 10: Test 4: mass (top), velocity (middle) and temperature (bottom). Results at time t_m using the the coupled ($\bullet$ for ions and $\times$ for electron) and the hydrodynamic (dashed line for ions and dotted line for electrons) solvers.

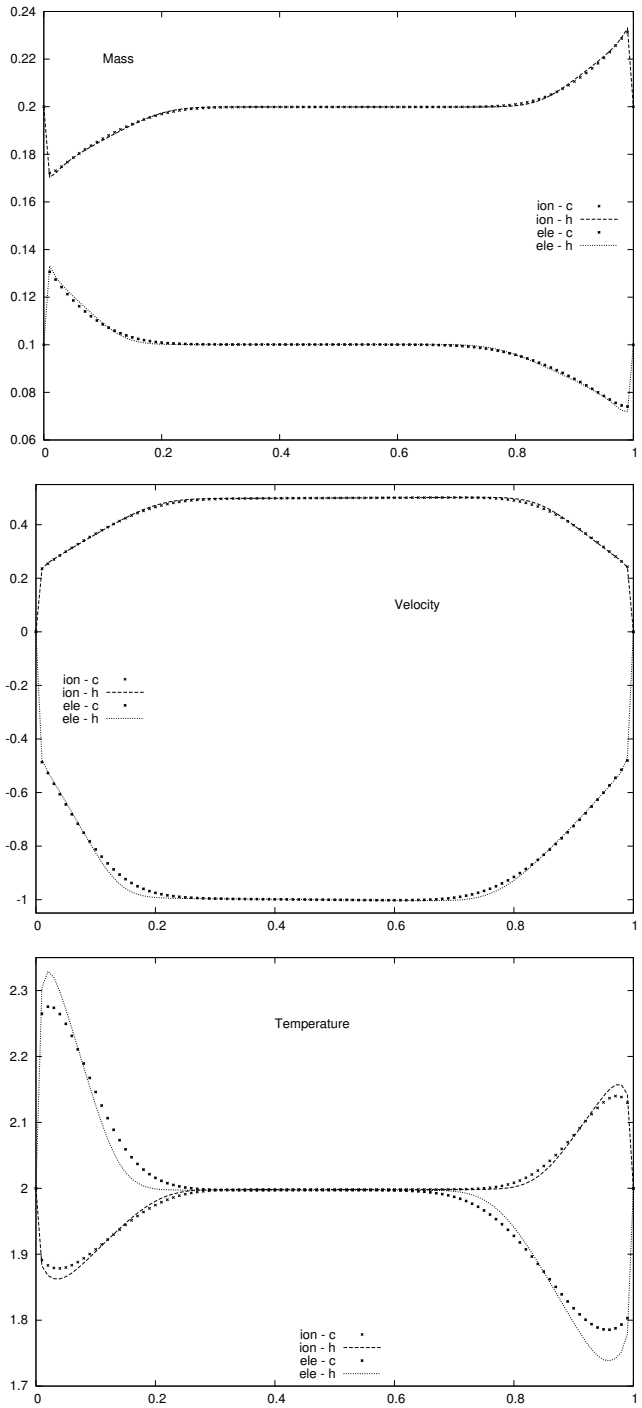

Figure 11: Test 4: mass (top), velocity (middle) and temperature (bottom). Results at time t_f using the the coupled ($\bullet$ for ions and $\times$ for electron) and the hydrodynamic (dashed line for ions and dotted line for electrons) solvers.

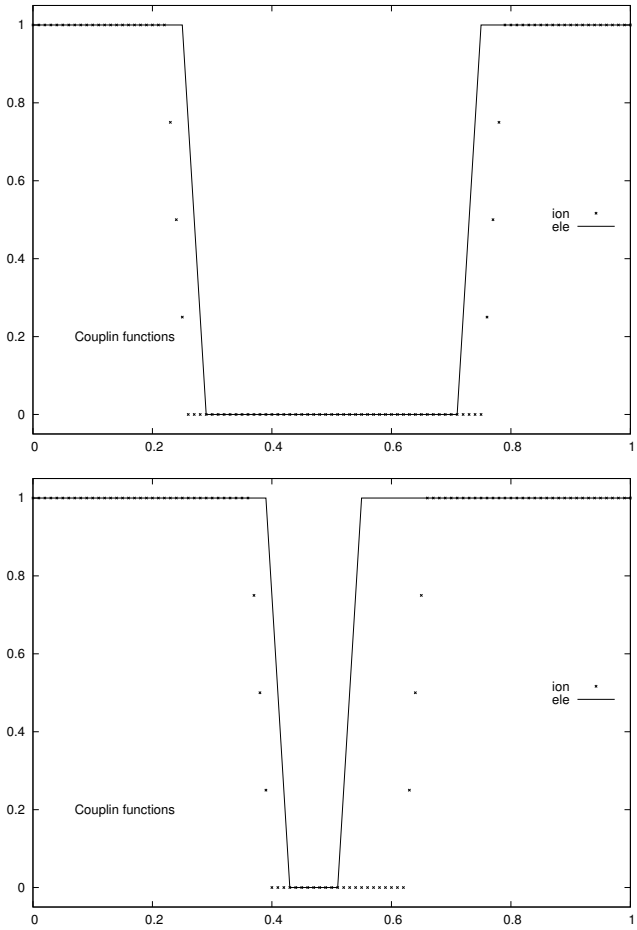

Figure 12: Test 4: coupling distribution functions for electrons (line) and ions (dots) at times t_m (top) and t_f (bottom).